IEEE Access
Multidisciplinary ⋮ Rapid Review ⋮ Open Access Journal

Received December 5, 2019, accepted December 21, 2019, date of publication December 30, 2019,
date of current version January 6, 2020.

Digital Object Identifier 10.1109/ACCESS.2019.2962302

Control of a Multivariable System Using Optimal Control Pairs: A Quadruple-Tank Process

PAVEL NAVRÁTIL[1], LIBOR PEKAŘ[1,2], AND RADEK MATUŠŮ[1,2]
[1]Department of Automation and Control Engineering, Faculty of Applied Informatics, Tomas Bata University in Zlín, 76005 Zlín, Czech Republic
[2]Centre for Security, Information and Advanced Technologies (CEBIA-Tech), Tomas Bata University in Zlín, 76001 Zlín, Czech Republic

Corresponding author: Libor Pekař (pekar@utb.cz)

This work was supported by the European Regional Development Fund under the project CEBIA-Tech Instrumentation No. CZ.1.05/2.1.00/19.0376 and by the Ministry of Education, Youth and Sports of the Czech Republic within the National Sustainability Programme project No. LO1303 (MSMT-7778/2014).

ABSTRACT This paper deals with one of the possible ways to control multivariable (MIMO) control loops. The suggested control design procedure uses the so-called primary controllers, auxiliary controllers, and also correction members. Parameters of the primary controllers are determined for the optimal control pairs using arbitrary single-variable synthesis methods; namely, the modulus optimum method, the balanced tuning method, and the desired model method. The optimal control pairs are determined using the so-called relative gain array tool or the relative normalized gain array tool combined with other tools, as the condition number or the Niederlinski index. The auxiliary feedback controllers serve for ensuring a control loop decoupling. Invariance to load disturbance of a control loop is realized by using the correction members. The novelty lies especially in the combination of the original inverted decoupling with disturbance rejection and provided tuning methods. The proposed control design for a MIMO loop is verified by simulation for the two-variable controlled plant of a quadruple-tank process and evaluated by using various criteria. Moreover, a numerical comparison to some other methods is given to the reader.

INDEX TERMS Control loop decoupling and invariance, multivariable control, optimal control pairs, quadruple-tank process, simulation.

I. INTRODUCTION

Controlled plants with one input variable and one output variable are classified as single-input single-output (SISO), or single-variable, ones. However, for a huge number of controlled plants, more than one output variable is controlled simultaneously via several input variables, i.e., input variables influence not only their corresponding output variables. These controlled plants are known as multi-input multi-output (MMO), or multivariable, ones and can be found in various areas of human activities, e.g. an air-condition system [1], [2], a tubular chemical reactor [3], [4], a military aircraft turbofan engine [5], a heating plant [6], a balance platform [7], an autopilot system [8], a quadcopter [9], [10], etc. The area of information technologies does not stand aside, MIMO systems can also be found in cloud computing [11]. It follows that MIMO control loops are complex and they consist of many mutually interconnected SISO control loops. A SISO control loop is a special case of a MIMO control loop [1], [12].

The associate editor coordinating the review of this manuscript and approving it for publication was Rathinasamy Sakthivel.

It is not easy to decide whether a simple structure of the control loop is sufficient to be used, or whether it is necessary to use a more complex structure of the control loop to MIMO plants. This means that it is desirable to know the structure and constraints of the whole control loop, i.e. the controlled plant, the controller, and the corresponding loop signals [13].

Decentralized control design represents one of possible framework approaches to control the MIMO plants [14]–[17]. By using decentralized control, independent feedback controllers are used to control a subset of input-output pairs [18]. The control problem is then separated into several independent single-loop SISO systems and then conventional SISO control is used on each of the loops [19], [20]. According to [18], [21], [22], the benefits of the use of decentralized controllers are, inter alia, as follows: easy implementation, efficient maintenance, simple tuning procedure due to fewer parameters to tune, or robustness to uncertainties.

A crucial step in the design of decentralized control systems is to determine input-output loop pairings (also called the control configuration selection) that have minimum cross-interactions among individual loops [17], [22]–[24]. A good closed-loop performance may not be achieved when an

improper input-output pairing is selected, even in the case of advanced and well-tuned controllers [25]. An unsuitable selection may even lead to closed-loop instability. That is to say, the input-output pairing yields a limitation of the loop interaction effect. Therefore, various pairing criteria (also called interaction measures) for a suitable control configuration selection were investigated during recent decades. Bristol [26] proposed a jointly-conditioned relative measure of input-output interactions called the relative gain array (RGA) based on the static gain matrix, which is not affected by scaling. In [27], its partially centralized block generalization – the so-called block gain array – was proposed, which gives better performance for highly interactive systems. For a control configuration with unsatisfactory performance, the partial RGA based on partially controlled feedback was suggested [28]. However, using the steady-state gain solely may lead to incorrect interaction measures [22]. Thus, the dynamic relative gain array (DRGA) [29], [30], or its extensions (the significant DRGA) [31] rather than RGA was introduced. Selecting the control configuration based on the DRGA magnitude may lead to a negative DRGA value and, consequently, to an incorrect pairing. Therefore, the effective RGA was proposed [32], combining the steady-state gain and bandwidth of the process transfer function element. To minimize overall loop interactions, the steady-state-based relative interaction array (RIA) [33], representing another interaction measure, was introduced. The normalized RGA (NRGA) introduced in [34] removes the RGA ambiguity of closeness to one. Based on the NRGA, He et al. [22] proposed the normalized relative gain array (RNGA) combining both the steady-state and the transient information for control configuration selection given by the average residence time. Balestrino *et al.* [35] designed the absolute RGA for solving both integrity problems and robustness to parameter variations and nonlinearity effects. Two input-output pairing strategies based on linear quadratic Gaussian control were suggested in [20], [36]. A mathematical pairing approach for square MIMO systems larger than 2×2 was proposed in [37]. An input-output pairing based on the solution of a multi-objective optimization problem was recently proposed [38]; this approach enables a systematic analysis of the conflict between the objectives and the performance of a control system. Last but not least, Kadhim [39] proposed a methodology combining RGA and RIA that determines whether the effect of gain uncertainty would invalidate the selected pairing. Besides the above-introduced results, many other pairing methods primarily not intended to decoupling control exist; for instance, those based on the Takagi-Sugeno fuzzy model [40] or the mutual information rate [41].

Even if suitable input-output pairs within decentralized the control configuration are selected, uncontrolled pairs are still coupled in general yielding residual cross-interactions. The idea of full decoupling control is that every single control loop has no interaction with another one. Otherwise, it is a partial coupling system [42], [43]. A MIMO control strategy can effectively be realized either by SISO decentralized controllers (with or without decouplers) or a centralized MIMO controller with decouplers [44], [45]. Decoupling algorithms can be divided into two categories: static decoupling and dynamic decoupling. A static decoupler can be designed based on the steady-state gain matrix [46]. Its implementation is generally simpler than that for a dynamic decoupler. However, it may not provide satisfactory decoupling performance in a closed-loop without non-integrative open loops. A dynamic decoupler, giving better performance in general, can provide the ideal decoupling, or a simplified decoupling, or it can be realized as an inverted decoupler [47]. The ideal (direct) decoupler attempts to obtain the open-loop serial connection of the decoupler and the control system diagonal with arbitrary transfer function matrix entries. Then, the controller can be assumed as a set of independent SISO controllers [48]. The ideal decoupling yields excellent performance; however, it can be sensitive to model uncertainties [49] and it has limited feasibility and applicability [50]. Simplified decoupling schemes provide less complex formulae compared to the ideal decoupler (e.g., some decoupler entries are set to one), which improves their applicability in practice [51]. On the other hand, the open-loop serial connection of the decoupler and the control system has a fixed form not allowing its parameterization. Therefore, controller tuning might not be easy [47]. A simple non-diagonal two-input two-output (TITO) decoupler was used to temperature control in [52]. Inverted decoupling [50], [53], [54], incorporating the decoupler or its part in a feedback-loop, has more benefits compared with other dynamic decoupling schemes (e.g., each decoupled loop can be kept away from acting as the secondary of other control loops, manual/automatic modes switching does not affect decoupling, easy construction of anti-wind-up schemes, etc.) [45], [54]; however, it cannot be used for non-minimum phase systems except for some special cases [55]. Different possible configurations of inverted decoupling strategy were proposed by Garrido *et al.* [56]. The inverted decoupler has been benchmarked and redesigned by many authors [57]–[59]. It was found that the systems with simplified decoupling are nominally stable, yet those with ideal and inverted decoupling are unstable, especially for non-minimum phase controlled systems [54]. If particular calculated decoupler elements are non-feasible or unstable, they can be additionally equipped with delays, extra dynamics or low-pass filters [60], [61]. Some authors proposed the design of MIMO centralized controllers implicitly or explicitly including the decoupling of control loops [58], [62]–[64]. Note that special ad-hoc decoupling schemes for systems with delays, nonlinear or complex systems, have also been proposed, see, e.g., [65]–[67]. Other modern techniques include, inter alia, bio-inspired [68], [69] adaptive [70], [71], fuzzy [72], [73], or neural network [74] decoupling control. The reader is referred to [45], [75] for further details.

Despite their simplicity, proportional-integral-derivative (PID) controllers still enjoy very high popularity among researchers and practitioners when designing a MIMO control loop. PIDs have been combined, e.g., with the

ideal [48], [76], a simplified [77], or an inverted [57] decoupling, a centralized control decoupler [62], [63], or decentralized control with a decoupling scheme based on the inverse Nyquist array [78].

The quadruple tank is another typical representative of the MIMO process [13], [79]–[82]. Various centralized [83], decentralized [60] control strategies or their comparisons [84] were published; however, a simplified decoupler was mostly used [60], [85]. Some researchers deservingly pointed out that non-minimum phase controlled plant operating points may occur here [81], [83], [85]. However, according to the authors' best knowledge, very few results introduced disturbances for this coupled-tank process and attempted to deal with their rejection or attenuation [60].

This study is aimed at the design of an inverted decentralized decoupling MIMO control strategy that, moreover, provides the ideal or a partial disturbance rejection. Note that it is assumed that the MIMO controlled plant has the same number of input and output variables. The proposed method utilizes selected tools that aid in determining the optimal control pairs for the MIMO controlled plant. Namely, the RGA and RNGA are used combined with the Niederlinski index (NI) [86] that represents an additional pairing rule to avoid a pairing yielding the feedback instability [20], [39]. In addition, the level of controllability is verified by using the condition number (CN) [87] making a decision about whether the controlled plant is ill-conditioned or not. The combination of RNGA and NI represents a sufficient optimal pairing condition in most cases [22], [88], and the triplet (with CN) constitutes a novelty. A link to the inverted decoupler [56] is discussed. As the proposed decoupling scheme or the computation of the term ensuring disturbance rejection (herein called as the correction members matrix) can yield a non-feasible result, compensation principles [61] are adopted to fix this issue. Once the decoupled controlled system is obtained, the primary controller of the PID type can be designed and tuned via an appropriate SISO synthesis method [89]–[91]. A note to the robust stability is given to the reader as well.

The second and also a substantial part of this study deals with an extensive comparative numerical example on control of a linearized model of the TITO four-tank process. Besides the proposed control strategy employing the optimal pairing, a non-optimal pairing, a simplified decoupler [45], [60], the standard inverted decoupler [56], an inverted fuzzy decoupler [73], a centralized inverted PI(D) decoupling control [64], [58], and a polynomial centralized coupled approach [92], [93] are compared by simulations. The results are evaluated by various criteria including integral ones; the designing specifics and limitations are assessed as well. They prove a very good performance of the proposed strategy, yet its deficiencies are discussed as well. Both a minimum phase and a non-minimum phase operating points are considered in the simulation example. The balanced tuning method (BTM) [94]–[96] is used to tune primary PID controllers for the minimum phase case, while the modulus optimum method (MOM) [97] is applied in the non-minimum phase case. For both the controlled plant models, the desired model method (DMM) [1] is used, in addition. Moreover, disturbance inputs are introduced and attenuated (even for a non-square transfer function matrices), which is widely neglected in the literature for the model as indicated above. Despite the fact that only the TITO model has been considered for the demonstration, the proposed techniques can be extended to a system with more variables, as discussed through the paper.

To sum up, the main contribution of this research lies in the unique combination of the optimal control configuration selection based on three indicators (which gives a sufficient optimal solution in most cases), the use of a novel inverted decoupler, the ideal (or a simplified) measurable disturbance elimination, and the used SISO controller tuning techniques. Moreover, the presented comprehensive numerical example of the four-tank process model control can highly be beneficial for the reader since it includes even a non-minimum phase case and disturbances rejection, and presents results for various control design principles.

II. ANALYSIS AND SYNTHESIS OF THE MULTI-VARIABLE CONTROL LOOP

A MIMO controlled plant consists of n output variables and m input variables; it is said that the plant is of $n \times m$ type. Note that, in this paper, it is considered that the number of inputs and outputs of the plant is the same, i.e., $m = n$, which means that it is of a square type.

A. BASIC DESCRIPTION OF THE MULTI-VARIABLE CONTROL LOOP

Assume a modified MIMO control loop scheme with measurable disturbance variables as in Fig. 1. In the figure, $\boldsymbol{U}(s)$ $[n \times 1]$ represents the Laplace transform of the manipulated variables vector, $\boldsymbol{V}(s)$ $[m \times 1]$ is the transformed vector of measurable disturbance variables, $\boldsymbol{W}(s)$ $[n \times 1]$ stands for the transformed vector of references (i.e., setpoints), and $\boldsymbol{E}(s)$ $[n \times 1]$ expresses the vector of control errors, i.e., $\boldsymbol{E}(s) = \boldsymbol{W}(s) - \boldsymbol{Y}(s)$. Matrices $\boldsymbol{G}_{SV}(s)$, $\boldsymbol{G}_{S}(s)$, $\boldsymbol{G}_{KC}(s)$, $\boldsymbol{G}_{R}(s)$, and $\boldsymbol{G}_{RP}(s)$ denote transfer function matrices of the disturbances to outputs, the controlled plant, the correction members, the primary controllers, and the auxiliary controllers, respectively. These matrices are considered in the following forms

$$\boldsymbol{G}_S(s) = \left[S_{ij}\right]_{n\times n}, \quad S_{ij} = \frac{Y_{S,i}(s)}{U_j(s)} \tag{1}$$

$$\boldsymbol{G}_{SV}(s) = \left[S_{Vij}\right]_{n\times m}, \quad S_{Vij} = \frac{Y_{SV,i}(s)}{V_j(s)} \tag{2}$$

$$\boldsymbol{G}_R(s) = \left[R_{ij}\right]_{n\times n}, \quad R_{ij} = \frac{U_{R,i}(s)}{E_j(s)} \tag{3}$$

$$\boldsymbol{G}_{KC}(s) = \left[KC_{ij}\right]_{n\times m}, \quad KC_{ij} = \frac{U_{KC,i}(s)}{V_j(s)} \tag{4}$$

$$\boldsymbol{G}_{RP}(s) = \left[RP_{ij}\right]_{n\times n}, \quad RP_{ij} = \frac{U_{RP,i}(s)}{U_{D,j}(s)} \tag{5}$$

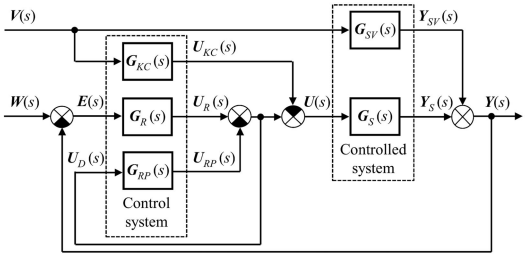

FIGURE 1. Modified scheme of multi-variable control loop with measurement of disturbance variables.

where $i, j \in \{1, 2, \ldots, n\}$ for (1), (3), (5), whereas $i \in \{1, 2, \ldots, n\}$, $j \in \{1, 2, \ldots, m\}$, $m \leq n$, for (2), (4).

Let us denote $\boldsymbol{U}(s) = [U_1(s), U_2(s), \ldots, U_n(s)]^T$, $\boldsymbol{Y}(s) = [Y_1(s), Y_2(s), \ldots, Y_n(s)]^T$, $[\boldsymbol{M}]_{ij}$ stands for the ijth element of a matrix $\boldsymbol{M}$, and $\boldsymbol{M}^{\mathrm{T}}$ is the matrix transpose.

B. DETERMINATION OF OPTIMAL CONTROL PAIRS

1) RELATIVE GAIN ARRAY (RGA)

The RGA represents the most common tool to determine the optimal control pairs for MIMO controlled plants; hence, it serves for the analysis of interactions between inputs and outputs [18], [19], [26]. The particular input-output interaction measure is represented by the value of the RGA matrix entry λ_{ij}

$$\boldsymbol{\Lambda} = \left[\lambda_{ij}\right]_{i\times j}, \quad i, j \in \{1, 2, \ldots, n\} \tag{6}$$

for which it holds that

$$\begin{aligned} \lambda_{ij} &= \frac{\lambda_{ij,num}}{\lambda_{ij,den}} = \frac{\left(\frac{\partial Y_i}{\partial U_j}\right)_{U_k}}{\left(\frac{\partial Y_i}{\partial U_j}\right)_{Y_l}} = \frac{[\boldsymbol{G}_S(s)]_{ij}}{\frac{1}{\left[\boldsymbol{G}_S^{-1}(s)\right]_{ji}}}, \\ U_k &= \text{const.}, \quad k \in \{1, 2, .., n\} \neq j, \\ Y_l &= \text{const.}, \quad l \in \{1, 2, .., n\} \neq i \end{aligned} \tag{7}$$

and

$$\sum_{i=1}^{n} \lambda_{ij} = \sum_{j=1}^{n} \lambda_{ij} = 1, \quad i \in \{1, 2, \ldots, n\}, \quad j \in \{1, 2, \ldots, n\} \tag{8}$$

see [19]. In (7), $\lambda_{ij,num}$ expresses the ratio between the output variable y_i and input variable u_j when all outputs are uncontrolled; i.e., it is the particular open-loop control gain (with all control loops opened). The value of $\lambda_{ij,den}$ is the ratio between the same output and input while all other output variables are perfectly controlled; in other words, it is the corresponding open-loop control gain with all other control loops closed.

The above description demonstrates the usefulness of the control configuration selection (i.e., the loop pairing). That is, if the feedback control of remaining outputs does not affect the particular input-output gain, it means that no interactions between loops are presented.

Elements of $\boldsymbol{\Lambda}$ can be determined as follows

$$\boldsymbol{\Lambda} = \boldsymbol{G}_S(s) \otimes \left(\boldsymbol{G}_S^{-1}(s)\right)^T \tag{9}$$

see [98], where $\otimes$ is the Schur product (or, the Hadamard product, i.e., the element-by-element multiplication). Although λ_{ij} are frequency-dependent, they are usually calculated for the zero frequency, i.e. the steady state, as follows

$$\boldsymbol{\Lambda}_0 = \boldsymbol{G}_S(0) \otimes \left(\boldsymbol{G}_S^{-1}(0)\right)^T = \boldsymbol{K} \otimes \boldsymbol{K} \tag{10}$$

where $\boldsymbol{K} = \boldsymbol{G}_S(0) = \left[k_{ij}\right]_{n\times n}$. Note that individual elements λ_{ij} are dimensionless and unaffected by scaling.

Optimal pairing decision rules using the RGA tool are recommended as follows [19], [20], [99]:

1) If $2/3 < \lambda_{ij} < 3/2$, the relation $u_j - y_i$ is suitable for pairing. Especially, the pairing is ideal (i.e., no interaction between the loops is presented).
2) If $\lambda_{ij} < 0$, the pair $u_j - y_i$ is extremely difficult to be controlled (i.e., it is highly undesirable).
3) If $\lambda_{ij} > 5$, the pairing y_i with u_j should be avoided (the interaction gets worse the larger λ_{ij} is).

To sum up, pairs are primarily found to satisfy condition 1) first. The remaining pairs are then determined such that they do not meet 2) or 3).

Example 1: Consider the RGA matrix $\boldsymbol{\Lambda}$ for a 3×3 controlled plant as

$$\boldsymbol{\Lambda} = \begin{bmatrix} 2/13 & 4/13 & 7/13 \\ 11/13 & 5/13 & -3/13 \\ 0/13 & 4/13 & 9/13 \end{bmatrix} \tag{11}$$

where the optimal control pairs are determined as follows, i.e., y_2-u_1, y_3-u_3, and y_1-u_2 (not y_1-u_3, even though it was the best option because input signal u_3 is already paired with the output signal y_3).

2) RELATIVE NORMALIZED GAIN ARRAY (RNGA)

The above mentioned RGA tool does not reflect the process dynamics. If the transfer function has a very long time constant compared to the others or large transport delays occur, the RGA may yield an incorrect recommendation. Hence, the RNGA tool can be used to determine the optimal control pairs taking the influence of process dynamics into account, rather than the RGA [22], [23].

The RNGA matrix $\boldsymbol{\Lambda}_N$, for the MIMO controlled plant $\boldsymbol{G}_S(s)$ is considered in the form

$$\boldsymbol{\Lambda}_N = \left[\lambda_{N,ij}\right]_{i\times j}, \quad i, j \in \{1, 2, \ldots, n\} \tag{12}$$

and defined as follows

$$\boldsymbol{\Lambda}_N = \left(\boldsymbol{G}_S(s) \odot \boldsymbol{T}_{AR}\right) \otimes \left(\boldsymbol{G}_S(s) \odot \boldsymbol{T}_{AR}\right)^{-T} \tag{13}$$

where $\odot$ denotes the element by element division and $\boldsymbol{T}_{AR} = [T_{AR,ij}]_{n\times n}$ is the average residence time matrix, for which holds that

$$T_{AR,ij} = \frac{1}{k_{ij}} \left| \int_0^\infty \left(h_{ij}(\infty) - h_{ij}(t)\right) \mathrm{d}t \right| \tag{14}$$

where k_{ij} and $h_{ij}(t)$ mean the static gain and the step response of the particular entry $S_{ij}(s)$ of $\boldsymbol{G}_S(s)$, respectively.

If it is assumed that $S_{ij}(s)$ has, in general, the following form

$$S_{ij}(s) = k_{ij} \frac{\prod_{r=1}^{m} \left(\tilde{T}_{ij,r} s + 1\right)}{\prod_{r=1}^{n} \left(T_{ij,r} s + 1\right)} \mathrm{e}^{-L_{ij} s}, \quad m < n \tag{15}$$

The value of $T_{AR,ij}$ can be approximated as

$$T_{AR,ij} = \left| \sum_{k=1}^{n} T_{ij,k} - \sum_{k=1}^{m} \tilde{T}_{ij,k} + L_{ij} \right| \tag{16}$$

see [1], [96].

In practice, the matrix Λ_N is calculated for the steady-state case as

$$\begin{aligned} \boldsymbol{\Lambda}_{N,0} &= (\boldsymbol{G}_S(0) \odot \boldsymbol{T}_{AR}) \otimes (\boldsymbol{G}_S(0) \odot \boldsymbol{T}_{AR})^{-T} \\ &= (\boldsymbol{K} \odot \boldsymbol{T}_{AR}) \otimes (\boldsymbol{K} \odot \boldsymbol{T}_{AR})^{-T} \\ &= \boldsymbol{K}_N \otimes \boldsymbol{K}_N^{-T} \end{aligned} \tag{17}$$

where $\boldsymbol{K}_N = [k_{N,ij}]_{n \times n}$ is the normalized gain matrix, in which

$$k_{N,ij} = \frac{k_{ij}}{T_{AR,ij}} \tag{18}$$

The optimal pairing decision rules are very close to those for the RGA matrix, i.e., it is recommended to set the control pair y_i-u_j for which $\lambda_{N,ij} \approx 1$ [100].

Example 2: Consider a MIMO controlled plant governed by the transfer function matrix

$$\boldsymbol{G}_S(s) = \begin{bmatrix} \dfrac{4(2s+1)}{(14s+1)(5s+1)} & \dfrac{-1}{3s+1}\mathrm{e}^{-s} \\ \dfrac{2}{s+1}\mathrm{e}^{-2s} & \dfrac{3}{(6s+1)^2}\mathrm{e}^{-10s} \end{bmatrix} \tag{19}$$

Then, the RGA matrix Λ according to (10) has the form

$$\boldsymbol{K} = \boldsymbol{G}_S(0) = \begin{bmatrix} 4 & -1 \\ 2 & 3 \end{bmatrix} \rightarrow \boldsymbol{\Lambda} = \begin{bmatrix} 0.8571 & 0.1429 \\ 0.1429 & 0.8571 \end{bmatrix} \tag{20}$$

which implies that the recommended control pairs via the RGA are y_1-u_1, y_2-u_2. However, the non-diagonal elements of (20) give faster responses than the diagonal ones due to their time constants. This fact is reflected by the RNGA matrix Λ_N

$$\begin{aligned} \boldsymbol{K}_N &= \boldsymbol{K} \odot \boldsymbol{T}_{AR} = \begin{bmatrix} 4 & -1 \\ 2 & 3 \end{bmatrix} \odot \begin{bmatrix} 17 & 4 \\ 3 & 22 \end{bmatrix} \\ &= \begin{bmatrix} 0.2353 & -0.2500 \\ 0.6667 & 0.1364 \end{bmatrix} \\ \rightarrow \boldsymbol{\Lambda}_{N,0} &= \begin{bmatrix} 0.1614 & 0.8386 \\ 0.8386 & 0.1614 \end{bmatrix} \end{aligned} \tag{21}$$

see (17), i.e., the eventual optimal control pairs determined via the RNGA are y_1-u_2, y_2-u_1.

3) NIEDERLINSKI INDEX AND CONDITION NUMBER

The NI [86] and CN [102] values represent addition rules that can be used for the analysis of interactions in MIMO controlled plants.

The NI is applied to analyze the stability of the proposed control loop structure for the selected optimal control configuration. This value is calculated for an $n \times n$ controlled plant $\boldsymbol{G}_S(s)$ (in the steady state) by using the following formula

$$NI = \frac{\det(\boldsymbol{G}_S(0))}{\prod_{i=1}^{n} S_{ii}(0)} = \frac{\det(\boldsymbol{K})}{\prod_{i=1}^{n} k_{ii}} \tag{22}$$

where $\det(\boldsymbol{G}_S(0))$ denotes the determinant of matrix $\boldsymbol{G}_S(0)$.

A negative NI value indicates instability in the proposed control structure. Then, the determined optimal input-output pairs are to be reordered such that their corresponding elements lie on the diagonal of $\boldsymbol{G}_S(s)$.

Remark 1: Example 2 refers to the advantage of using RNGA rather than RGA. Moreover, it was shown that loop paring based on the combination of RGA and NI criteria is necessary and sufficient condition only for TITO systems and it becomes (only) a necessary condition for higher dimensional systems [88], [101]. This obstacle is overcome by the use of RNGA plus NI control configuration selection [22].

The CN is a measure of the sensitivity of the matrix properties to changes in its individual elements and it serves to decide about the controllability of the MIMO plant. It is defined as the ratio of the largest to the smallest gains of the MIMO controlled plant. These gains cannot be determined simply as particular SISO controlled plant gains because the input and the output signals are vectors and do not have only the size but also the direction. They depend on the frequency and the direction of the input vector and are expressed by means of singular values $\boldsymbol{G}_S(s)$ as follows

$$CN = \frac{\sigma_{\max}\left([\boldsymbol{G}_S(s)]_{s=\mathrm{j}\omega}\right)}{\sigma_{\min}\left([\boldsymbol{G}_S(s)]_{s=\mathrm{j}\omega}\right)} \tag{23}$$

where

$$\sigma_i = \sqrt{\mathrm{eig}\left(\left([\boldsymbol{G}_S(s)]_{s=\mathrm{j}\omega}\right)^H \left([\boldsymbol{G}_S(s)]_{s=\mathrm{j}\omega}\right)\right)} \tag{24}$$

for $i = 1, 2, \ldots, r$, where r stands for the rank of $\left([\boldsymbol{G}_S(s)]_{s=\mathrm{j}\omega}\right)^H \left([\boldsymbol{G}_S(s)]_{s=\mathrm{j}\omega}\right)$, the superscript H denotes Hermitian transpose, $\omega$is a particular frequency, and $\sigma_{\max}$, $\sigma_{\min}$ are, respectively, maximum and minimum singular values of matrix $[\boldsymbol{G}_S(s)]_{s=\mathrm{j}\omega}$ [87], [103].

Since ill-conditioned plants may be hard to control, it is of importance to avoid control systems with large CN. Namely, if CN < 10, the controlled plant can be decoupled, i.e., it is possible to determine the optimal control pairs. Otherwise, the plant is difficult to control due to the ill-conditioned matrix $[\boldsymbol{G}_S(s)]_{s=\mathrm{j}\omega}$ [51]. Moreover, the CN is closely related to the RGA, see [101] for further details.

To sum up, the optimal control configuration selection can be determined by using the mentioned tools or their combinations (e.g., the CN with the RGA [87], the RGA,

the RNGA with the NI [100]). However, the final decision can then be made not only via described tools but also based on further physical reasoning and experience of the reader [102]. Due to Remark 1, we herein eventually use the RNGA plus NI, supported by CN, which is a novel combination.

Hereinafter, we do let call S_{ij} of (1) corresponding to the optimally paired inputs and outputs as dominant.

C. ELIMINATION OF DISTURBANCE VARIABLES AND LOOP INTERACTION EFFECTS IN A MULTI-VARIABLE CONTROL LOOP

Except for reaching the stability of the MIMO control loop and its performance, it is often necessary to satisfy the decoupling; i.e., to eliminate the control loops interactions. The elimination or attenuation of the effect of measurable disturbances on controlled variables constitutes another possible synthesis goal. Then, the control loop is called absolutely invariant if the influence of the disturbance variables is completely (ideally) eliminated. Otherwise, the loop is approximately invariant (for instance, the invariance is asymptotic, i.e. in a steady state).

Consider the control system as in Fig. 1. Then, the following transfer function matrices can be assembled

$$\begin{aligned} \boldsymbol{G}_{W/Y}(s) &= \left[\boldsymbol{I}+\boldsymbol{G}_S(s)\left(\boldsymbol{I}+\boldsymbol{G}_{RP}(s)\right)^{-1}\boldsymbol{G}_R(s)\right]^{-1} \\ &\quad\cdot \boldsymbol{G}_S(s)\left(\boldsymbol{I}+\boldsymbol{G}_{RP}(s)\right)^{-1}\boldsymbol{G}_R(s) \qquad (25) \\ \boldsymbol{G}_{V/Y}(s) &= \left[\boldsymbol{I}+\boldsymbol{G}_S(s)\left(\boldsymbol{I}+\boldsymbol{G}_{RP}(s)\right)^{-1}\boldsymbol{G}_R(s)\right]^{-1} \\ &\quad\cdot \left[\boldsymbol{G}_{SV}(s)-\boldsymbol{G}_S(s)\boldsymbol{G}_{KC}(s)\right] \qquad (26) \end{aligned}$$

for which it holds that

$$\boldsymbol{Y}(s)=\boldsymbol{G}_{W/Y}(s)\boldsymbol{W}(s)+\boldsymbol{G}_{V/Y}(s)\boldsymbol{V}(s) \qquad (27)$$

1) DECOUPLING

The auxiliary MIMO feedback-loop controller $\boldsymbol{G}_{RP}(s)$ is used to ensure the decoupling. The proposed decoupling scheme is inspired by an analogy to the transition from open-loop to feedback-loop control. Hence, instead of the use of an open-loop decoupler (ideal or simplified one), we attempt to use it in a feedback structure to enhance stability issues and response to disturbances. A general inverse decoupler has some other advantages, as reviewed in Introduction.

The goal of the proposed method is to achieve the resulting controlled open loop $\boldsymbol{H}(s)$ of (25) with $\boldsymbol{G}_{RP}(s)$ equal to $\boldsymbol{G}_S(s)$ in which all non-paired transfer functions are

$$\boldsymbol{H}(s)=\boldsymbol{G}_S(s)\left(\boldsymbol{I}+\boldsymbol{G}_{RP}(s)\right)^{-1}\stackrel{!}{=}\boldsymbol{G}_S(s)\otimes\boldsymbol{M} \qquad (28)$$

where

$$\begin{aligned} [\boldsymbol{M}]_{i,j} &= 1 \quad \text{for dominant } S_{ij} \\ [\boldsymbol{M}]_{i,j} &= 0 \quad \text{for non-dominant } S_{ij} \end{aligned} \qquad (29)$$

Conditions (28), (29) are satisfied by applying the following relations

$$\begin{aligned} RP_{ij} &= \frac{S_{kj}}{\tilde{S}_{ki}} \neq 0 \quad \text{for } i \neq j, \\ RP_{ij} &= 0 \quad \text{for } i=j,\ i,j,k \in \{1,2,\ldots,n\} \end{aligned} \qquad (30)$$

where S_{kj} represent the non-dominant (unpaired) entries of $\boldsymbol{G}_S(s)$, whereas $\tilde{S}_{ki}$ are the dominant (paired) ones in the k-th row.

Remark 2: For a given i in (30), the formula requires to search for the dominant element of $\boldsymbol{G}_S(s)$ in its i-th column, which gives rise to the particular k-th row. It is worth noting that conditions (30) have been derived by the Symbolic toolbox in Matlab up to the 5×5 MIMO system. A proof for a system with an arbitrary dimension is a matter of future research. The solution of (28) reads

$$RP_{ij}=\frac{S_{kj}}{\tilde{S}_{ki}}\left(1+RP_{ii}\right) \quad \text{for } i \neq j, \qquad (31)$$

Hence, we do let set RP_{ii} to zero for simplicity, which yields (30). Example 3 elucidates the calculation of $\boldsymbol{G}_{RP}(s)$ for a general 3×3 system.

Example 3: Consider a MIMO controlled plant governed by the transfer function matrix

$$\boldsymbol{G}_S(s)=\begin{bmatrix} S_{11} & S_{12} & S_{13} \\ S_{21} & S_{22} & S_{23} \\ S_{31} & S_{32} & S_{33} \end{bmatrix} \qquad (32)$$

Let $\tilde{S}_{12}=S_{12}, \tilde{S}_{23}=S_{23}, \tilde{S}_{31}=S_{31}$, then (30) gives

$$\boldsymbol{G}_{RP}(s)=\begin{bmatrix} 0 & \frac{S_{32}}{\tilde{S}_{31}} & \frac{S_{33}}{\tilde{S}_{31}} \\ \frac{S_{11}}{\tilde{S}_{12}} & 0 & \frac{S_{13}}{\tilde{S}_{12}} \\ \frac{S_{21}}{\tilde{S}_{23}} & \frac{S_{22}}{\tilde{S}_{23}} & 0 \end{bmatrix} \qquad (33)$$

One can verify that

$$\begin{aligned} \boldsymbol{H}(s) &= \boldsymbol{G}_S(s)\left(\boldsymbol{I}+\boldsymbol{G}_{RP}(s)\right)^{-1} \\ &= \boldsymbol{G}_S(s)\otimes\begin{bmatrix} 0 & 1 & 0 \\ 0 & 0 & 1 \\ 1 & 0 & 0 \end{bmatrix} = \begin{bmatrix} 0 & S_{12} & 0 \\ 0 & 0 & S_{23} \\ S_{31} & 0 & 0 \end{bmatrix} \end{aligned} \qquad (34)$$

which enables us to set three independent SISO controllers for the optimal pairs y_1-u_2, y_2-u_3, y_3-u_1.

If fractions in (30) give some unstable or non-feasible elements of $\boldsymbol{G}_{RP}(s)$ – e.g., due to input-output delays or a negative relative order – one can adopt the following recommendation [61] that uses a compensation element

$$\begin{aligned} RP_{ij} &\rightarrow RP_{ij}\cdot C_{ij} \\ C_{ij} &= \mathrm{e}^{-\alpha s}\prod_{i=1}^{n}\frac{(s-s_i)^{n_i}}{(-s-s_i)^{n_i}}\frac{1}{f(s)} \end{aligned} \qquad (35)$$

where $\alpha > 0$ (to compensate for a negative delay), s_i stands for a right-half plane (RHP) pole of RP_{ij} with the multiplicity of n_i, and $f(s)$ is an appropriate polynomial acting as the inverse of a low-pass filter to get a non-negative relative degree of RP_{ij}. Note that the question of feasibility or stability of systems with delays in its dynamics [104] goes far beyond this work and it is to be solved within the

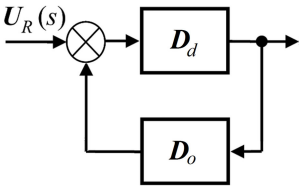

FIGURE 2. The classic inverted decoupling scheme [56].

future research. However, the use of (35) destroys the ideal decoupling.

Remark 3: The independently proposed inverse decoupler resembles the classic inverse decoupler [56] depicted in Fig. 2. However, there are some essential differences between the approaches. The proposed method gives a unique explicit computational formula (30) with a single feedback element. On the other hand, an implicit expression is primarily provided by [56], the solution of which is, moreover, not straightforward due to the existence of multiple solutions and it requires the user's erudition and experience. In more detail, the transfer function matrix of the serial link of the inverted decoupler and the controlled system reads

$$\boldsymbol{G}_S(s)\,\boldsymbol{D}_d(s)\left(\boldsymbol{I}-\boldsymbol{D}_o(s)\,\boldsymbol{D}_d(s)\right)^{-1} \tag{36}$$

The goal is to set (36) equal to the desired transfer function matrix of the apparent process $\boldsymbol{H}_a(s)$, which gives rise to the implicit condition

$$\boldsymbol{D}_d^{-1}(s)-\boldsymbol{D}_o(s)=\boldsymbol{H}_a^{-1}(s)\,\boldsymbol{G}_S(s) \tag{37}$$

Assume the same condition as in (28), i.e., $\boldsymbol{H}_a(s) = \boldsymbol{G}_S(s)\otimes\boldsymbol{M}$. Then, in the case of a TITO process with the diagonal $\boldsymbol{M}(s)$, (37) has two solutions denoted as 1-2 and 2-1 configurations, given by (38) and (39), respectively.

$$\boldsymbol{D}_{d,1-2}(s)=\boldsymbol{I},\quad \boldsymbol{D}_{o,1-2}(s)=\begin{bmatrix}0 & -\dfrac{S_{12}}{S_{11}}\\ -\dfrac{S_{21}}{S_{22}} & 0\end{bmatrix} \tag{38}$$

$$\boldsymbol{D}_{d,2-1}(s)=\begin{bmatrix}0 & -\dfrac{S_{22}}{S_{21}}\\ -\dfrac{S_{11}}{S_{12}} & 0\end{bmatrix},\quad \boldsymbol{D}_{o,2-1}(s)=\boldsymbol{I} \tag{39}$$

Note that if $\boldsymbol{M}(s)$ is off-diagonal, then 1-2 and 2-1 configurations read, respectively,

$$\boldsymbol{D}_{d,1-2}(s)=\boldsymbol{I},\quad \boldsymbol{D}_{o,1-2}(s)=\begin{bmatrix}0 & -\dfrac{S_{22}}{S_{21}}\\ -\dfrac{S_{11}}{S_{12}} & 0\end{bmatrix} \tag{40}$$

$$\boldsymbol{D}_{d,2-1}(s)=\begin{bmatrix}0 & -\dfrac{S_{12}}{S_{11}}\\ -\dfrac{S_{21}}{S_{22}} & 0\end{bmatrix},\quad \boldsymbol{D}_{o,2-1}(s)=\boldsymbol{I} \tag{41}$$

By comparison of Fig. 1 with Fig. 2 and (30) with (38), it can easily be deduced that the proposed inverted decoupler agrees with the 1-2 configuration and

$$\boldsymbol{G}_{RP}(s)=-\boldsymbol{D}_{o,1-2}(s) \tag{42}$$

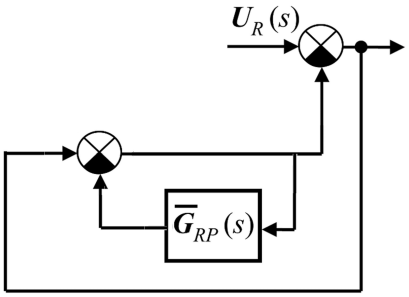

FIGURE 3. Proposed modified (nested) inverted decoupler.

The question is how to identify the proposed scheme with the 2-1 configuration. The solution is suggested in the following proposition.

Proposition 1: Let the proposed decoupling scheme be modified as in Fig. 3 with decoupler $\bar{\boldsymbol{G}}_{RP}(s)$. Then, this scheme agrees with the 2-1 configuration as follows

$$\bar{\boldsymbol{G}}_{RP}(s)=-\left(\boldsymbol{D}_{d,2-1}+\boldsymbol{D}_{o,2-1}\right) \tag{43}$$

Proof: According to Fig. 3, one can write the following transfer function matrix of the modified inverted (nested) decoupler

$$\left(\boldsymbol{I}+\left(\boldsymbol{I}+\bar{\boldsymbol{G}}_{RP}(s)\right)^{-1}\right)^{-1} \tag{44}$$

By comparison of (44) with (36)

$$\begin{aligned}\boldsymbol{D}_d(s)\left(\boldsymbol{I}-\boldsymbol{D}_o(s)\,\boldsymbol{D}_d(s)\right)^{-1}&=\left(\boldsymbol{I}+\left(\boldsymbol{I}+\bar{\boldsymbol{G}}_{RP}(s)\right)^{-1}\right)^{-1}\\ \left(\boldsymbol{I}-\boldsymbol{D}_o(s)\,\boldsymbol{D}_d(s)\right)\boldsymbol{D}_d^{-1}(s)&=\boldsymbol{I}+\left(\boldsymbol{I}+\bar{\boldsymbol{G}}_{RP}(s)\right)^{-1}\end{aligned} \tag{45}$$

Due to (38) and (42), one gets

$$\begin{aligned}\boldsymbol{I}+\boldsymbol{G}_{RP}(s)&=\boldsymbol{I}+\left(\boldsymbol{I}+\bar{\boldsymbol{G}}_{RP}(s)\right)^{-1}\\ \boldsymbol{G}_{RP}(s)&=\left(\boldsymbol{I}+\bar{\boldsymbol{G}}_{RP}(s)\right)^{-1}\\ \Rightarrow\bar{\boldsymbol{G}}_{RP}(s)&=\boldsymbol{G}_{RP}^{-1}(s)-\boldsymbol{I}\end{aligned} \tag{46}$$

Yet, from (38), (39) and (42), it can be deduced that

$$\boldsymbol{G}_{RP}^{-1}(s)=-\boldsymbol{D}_{o,1-2}^{-1}(s)=-\boldsymbol{D}_{o,2-1}(s) \tag{47}$$

which, eventually, yields (43). The derivation of (43) for (40) and (41) can be done analogously. ■

The nested decoupler (or, equivalently the 2-1 configuration) can be used whenever the originally proposed inverted decoupler (or, the 1-2 configuration) gives some non-feasible decoupler entries. However, even if such a case can be partially solved by (35), the solution then provides a non-ideal decoupling.

Once the decoupling procedure is finished, individual entries R_{ij} of $\boldsymbol{G}_R(s)$ can be then determined. If the decoupling is ideal, i.e. if (28) holds, the primary controllers can be calculated solely based on the corresponding optimally paired (i.e., dominant) elements of $\boldsymbol{G}_S(s)$. In this case, let us denote a modified open loop $\bar{\boldsymbol{H}}(s) = \boldsymbol{H}_a(s) = \boldsymbol{G}_S(s)\otimes\boldsymbol{M}$.

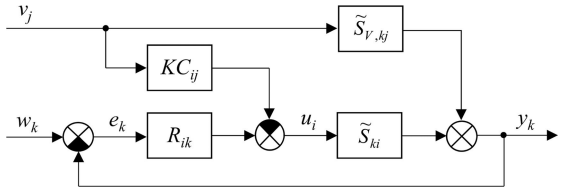

FIGURE 4. Single-variable branched control loops with disturbance variables measurement for approximate invariance.

Otherwise, the modified open-loop controlled system has to be determined via

$$\bar{\boldsymbol{H}}(s) = \boldsymbol{H}(s) \otimes \boldsymbol{M} = \boldsymbol{G}_S(s)\,(\boldsymbol{I} + \boldsymbol{G}_{RP}(s))^{-1} \otimes \boldsymbol{M} \tag{48}$$

Then, the primary controllers are calculated as follows

$$\begin{aligned} R_{ij} &\neq 0 \quad \text{for non-zero entries of } \left[\bar{\boldsymbol{H}}(s)\right]_{ji}, \\ R_{ij} &= 0 \quad \text{for zero entries of } \left[\bar{\boldsymbol{H}}(s)\right]_{ji}, \\ & i, j \in \{1, 2, \ldots, n\} \end{aligned} \tag{49}$$

2) INVARIANCE

Absolute invariance (or, the ideal disturbance rejection) of the MIMO control loop is satisfied if the disturbance transfer function matrix $\boldsymbol{G}_{V/Y}(s)$ (26) is equal to zero matrix, i.e., if the following relation holds

$$\boldsymbol{G}_{KC}(s) = \boldsymbol{G}_S^{-1}(s)\,\boldsymbol{G}_{SV}(s) \tag{50}$$

Formula (50) can also be formulated using entries of $\boldsymbol{G}_{KC}(s)$ as

$$\begin{aligned} KC_{ij} &= \frac{1}{\det(\boldsymbol{G}_S(s))} \sum_{k=1}^{n} s_{ki} \cdot S_{V,kj}, \\ \det(\boldsymbol{G}_S(s)) &\neq 0, \quad i \in \{1, 2, \ldots, n\}, \\ & j \in \{1, 2, \ldots, m\}, \quad m \leq n \end{aligned} \tag{51}$$

where $\det(\boldsymbol{G}_S(s))$ denotes the determinant of $\boldsymbol{G}_S(s)$, $S_{V,kj}$ are particular entries of $\boldsymbol{G}_{SV}(s)$, and s_{ki} represent cofactors (algebraic adjuncts) of $\boldsymbol{G}_S(s)$.

Regarding approximate (non-ideal) invariance of the MIMO control loop, SISO branched control loops with disturbance variables measurement can be used, see Fig. 4 [1]. Correction members KC_{ij} are then determined solely by using the dominant (optimally paired) entries of $\boldsymbol{G}_S(s)$ and $\boldsymbol{G}_{SV}(s)$. The influence of the remaining (i.e., non-dominant) entries of $\boldsymbol{G}_S(s)$ and $\boldsymbol{G}_{SV}(s)$ is omitted. As a result, the optimal pairs v_j-y_k are rejected only. Note that techniques introduced in Subsection II.B are used to verify the influence of individual elements of $\boldsymbol{G}_{SV}(s)$.

The designing rules are

$$\begin{aligned} KC_{ij} &= \frac{\tilde{S}_{V,kj}}{\tilde{S}_{ki}} \quad i, k \in \{1, 2, \ldots, n\},\ j \in \{1, 2, \ldots, m\}, \\ & \qquad m \leq n, \\ KC_{ij} &= 0 \text{ for remaining correction members of } \boldsymbol{G}_{KC}(s) \end{aligned} \tag{52}$$

where $\tilde{S}_{V,kj}$ and $\tilde{S}_{ki}$ represent, respectively, the dominant elements of $\boldsymbol{G}_{SV}(s)$ and $\boldsymbol{G}_S(s)$ in the k-th row.

It holds again that if (50) or (52) yields some non-feasible transfer functions, compensator (35) can be utilized.

D. ROBUST STABILITY ANALYSIS

We do let concisely provide the reader with a general possibility of how to verify the robust stability of the proposed MIMO control loop in this subsection. Robustness analysis is an important aspect of the control system due to unmodeled process dynamics in real-world systems.

Consider the input and the output multiplicative uncertainties of the controlled plant, respectively,

$$\begin{aligned} \widehat{\boldsymbol{G}}_{S,in}(s) &= \boldsymbol{G}_S(s)\,(\boldsymbol{I} + \boldsymbol{\Delta}_{in}(s)) \\ \widehat{\boldsymbol{G}}_{S,out}(s) &= (\boldsymbol{I} + \boldsymbol{\Delta}_{out}(s))\,\widehat{\boldsymbol{G}}_S(s) \end{aligned} \tag{53}$$

where $\boldsymbol{G}_S(s)$ stands for the nominal model, whereas $\widehat{\boldsymbol{G}}_{S,in}(s)$, $\widehat{\boldsymbol{G}}_{S,out}(s)$ represent perturbed ones. The control system is robustly stable according to the small gain theorem and the spectral radius stability [102] if the following constraints conditions hold

$$\begin{aligned} \|\boldsymbol{T}_{in}(s)\,\boldsymbol{\Delta}_{in}(s)\|_\infty < 1 \Leftrightarrow \rho(-\boldsymbol{T}_{in}(\mathrm{j}\omega)\,\boldsymbol{\Delta}_{in}(\mathrm{j}\omega)) < 1, \\ \omega \in [0, \infty) \\ \|\boldsymbol{T}_{out}(s)\,\boldsymbol{\Delta}_{out}(s)\|_\infty < 1 \Leftrightarrow \rho(-\boldsymbol{T}_{out}(\mathrm{j}\omega)\,\boldsymbol{\Delta}_{out}(\mathrm{j}\omega)) < 1, \\ \omega \in [0, \infty) \end{aligned} \tag{54}$$

where, respectively,

$$\begin{aligned} \boldsymbol{T}_{in}(s) &= -(\boldsymbol{I} + \boldsymbol{G}_{RP}(s))^{-1}\,\boldsymbol{G}_R(s) \\ &\quad \cdot \left[\boldsymbol{I} + \boldsymbol{G}_S(s)\,(\boldsymbol{I} + \boldsymbol{G}_{RP}(s))^{-1}\,\boldsymbol{G}_R(s)\right]^{-1} \boldsymbol{G}_S(s) \\ \boldsymbol{T}_{out}(s) &= -\boldsymbol{G}_S(s)\,(\boldsymbol{I} + \boldsymbol{G}_{RP}(s))^{-1}\,\boldsymbol{G}_R(s) \\ &\quad \cdot \left[\boldsymbol{I} + \boldsymbol{G}_S(s)\,(\boldsymbol{I} + \boldsymbol{G}_{RP}(s))^{-1}\,\boldsymbol{G}_R(s)\right]^{-1} \end{aligned} \tag{55}$$

The above-introduced conditions (54) can also be expressed graphically by identifying whether particular the magnitude plots go below 1 for some frequency value.

Thus, one can determine the multiplicative uncertainties for the controlled plant and then use (54) to decide about the robust stability. It is worth noting that perturbations in $\boldsymbol{G}_{SV}(s)$ do not affect the robust stability.

E. MULTI-VARIABLE CONTROL LOOP SYNTHESIS SUMMARY

The herein proposed approach to control the MIMO loops is summarized in this subsection. The basic design steps are as follows:

1) The optimal control pairs are determined by using the analysis of the interactions between inputs and outputs in the given MIMO controlled plant, as described in Subsection II.B.
2) The auxiliary controllers RP_{ij} in $\boldsymbol{G}_{RP}(s)$ are set according to (30) and (35) (if needed) to get the decoupled

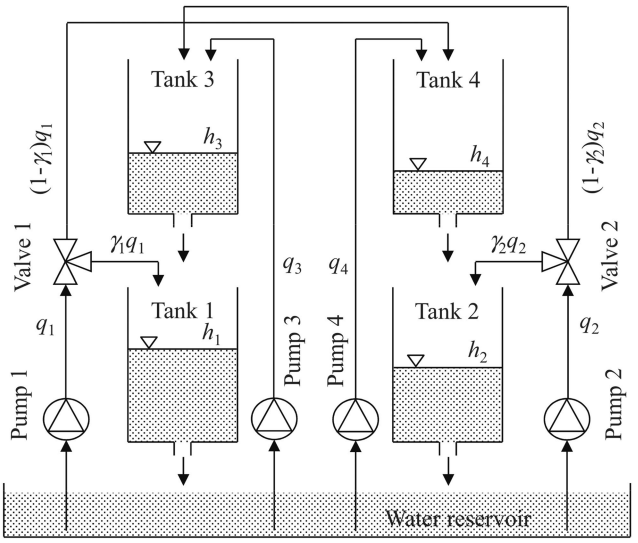

FIGURE 5. Schematic diagram of (two-variable) quadruple-tank controlled plant.

MIMO control loop. Note that for a TITO case, setting (43) can alternatively be used.

3) Parameters of the primary controllers R_{ij} in $\boldsymbol{G}_R(s)$ are calculated in accordance to (49) via an arbitrary SISO synthesis method.
4) The correction members KC_{ij} in $\boldsymbol{G}_{KC}(s)$ are set using (50) or (52) to get the absolute or an approximate invariance to disturbances, respectively.

Hereinafter, it is considered that matrices $\boldsymbol{G}_S(s)$ and $\boldsymbol{G}_{SV}(s)$ are of the TITO (i.e., 2×2) type

$$\boldsymbol{G}_S(s) = \begin{bmatrix} S_{11} & S_{12} \\ S_{21} & S_{22} \end{bmatrix}, \quad \boldsymbol{G}_{SV}(s) = \begin{bmatrix} S_{V11} & S_{V12} \\ S_{V21} & S_{V22} \end{bmatrix} \tag{56}$$

for which holds that

$$\boldsymbol{Y}(s) = \boldsymbol{G}_S(s)\,\boldsymbol{U}(s) + \boldsymbol{G}_{SV}(s)\,\boldsymbol{V}(s) \tag{57}$$

III. SIMULATION EXAMPLE: A QUADRUPLE TANK

A. QUADRUPLE-TANK PROCESS DESCRIPTION AND MODEL

Examples of MIMO control plants can also be found in the reign of hydraulic systems and processes [87], [102]. The quadruple tank (the schematic diagram of which is displayed in Fig. 5) is a widely used representative of such systems [13], [60], [79]–[85], that can be described by a TITO model with two disturbance variables.

In Fig. 5, h_1 to h_4 are water levels of the corresponding tanks, γ_1, γ_2 represent ratios of mass flows through the corresponding valves, and q_1 to q_4 are mass flows through the corresponding pumps. These physical quantities of the process represent general input/output variables of a MIMO system as in Fig. 1. Namely, manipulated variables (u_i) are represented by q_1, q_2, controlled variables (y_i) are represented by h_1, h_2, and disturbance variables (v_i) are represented by q_3, q_4.

TABLE 1. Parameter values of the quadruple tank appliance.

Parameter	A_1, A_3 [cm^2]	A_2, A_4 [cm^2]	a_1, a_3 [cm^2]	a_2, a_4 [cm^2]	g [cm·s^{-2}]
Value	28	32	0.071	0.057	981

1) MATHEMATICAL MODEL OF THE PROCESS

Mass balances and Bernoulli's law yield a nonlinear mathematical model of the controlled plant described by the following differential equations

$$\begin{aligned}
\frac{\mathrm{d}h_1(t)}{\mathrm{d}t} &= -\frac{a_1}{A_1}\sqrt{2gh_1(t)} + \frac{a_3}{A_1}\sqrt{2gh_3(t)} + \frac{\gamma_1}{A_1}q_1(t) \\
\frac{\mathrm{d}h_2(t)}{\mathrm{d}t} &= -\frac{a_2}{A_2}\sqrt{2gh_2(t)} + \frac{a_4}{A_2}\sqrt{2gh_4(t)} + \frac{\gamma_2}{A_2}q_2(t) \\
\frac{\mathrm{d}h_3(t)}{\mathrm{d}t} &= -\frac{a_3}{A_3}\sqrt{2gh_3(t)} + \frac{(1-\gamma_2)}{A_3}q_2(t) + \frac{1}{A_3}q_3(t) \\
\frac{\mathrm{d}h_4(t)}{\mathrm{d}t} &= -\frac{a_4}{A_4}\sqrt{2gh_4(t)} + \frac{(1-\gamma_1)}{A_4}q_1(t) + \frac{1}{A_4}q_4(t)
\end{aligned} \tag{58}$$

where A_i and a_i are cross-section areas of the ith tank and its outlet hole, respectively, and g denotes the gravitational acceleration. It is considered the height of each tank is 20cm, a capacity of pumps 1, 2 is about 40cm^3 s^{-1} and pumps 3, 4 about 10 cm^{3}s^{-1}. Other physical values of these parameters for the laboratory appliance are given in Table 1 [13].

2) MODEL LINEARIZATION

The first-order Taylor expansion applied to model (58) can generally be expressed as

$$\begin{aligned}
f_k\left(h_i, q_j\right)(t) &= \frac{\mathrm{d}h_k(t)}{\mathrm{d}t} = \dot{h}_k(t) \\
&\approx f_k(h_i^0, q_j^0) + \sum_{i=1}^{4} \left.\frac{\partial f_k\left(h_i, q_j\right)(t)}{\partial h_i(t)}\right|_{h_i=h_i^0} \Delta h_i(t) \\
&\quad + \sum_{j=1}^{4} \left.\frac{\partial f_k\left(h_i, q_j\right)(t)}{\partial q_j(t)}\right|_{q_j=q_j^0} \Delta q_j(t)
\end{aligned} \tag{59}$$

where $i, j, k \in \{1, 2, 3, 4\}$, the doublet $\left\{h_i^0, q_j^0\right\}$ represents a stationary operating point of (59), $\Delta h_i(t) = h_i(t) - h_i^0$, and $\Delta q_j(t) = q_j(t) - q_j^0$. Then, particular linearized equations read

$$\begin{aligned}
\Delta\dot{h}_1(t) &= -\frac{a_1}{A_1}\sqrt{\frac{g}{2h_1^0}}\Delta h_1(t) + \frac{a_3}{A_1}\sqrt{\frac{g}{2h_3^0}}\Delta h_3(t) \\
&\quad + \frac{\gamma_1}{A_1}\Delta q_1(t) \\
\Delta\dot{h}_2(t) &= -\frac{a_2}{A_2}\sqrt{\frac{g}{2h_2^0}}\Delta h_2(t)\,\frac{a_4}{A_2}\sqrt{\frac{g}{2h_4^0}}\Delta h_4(t) \\
&\quad + \frac{\gamma_2}{A_2}\Delta q_2(t)
\end{aligned}$$

$$\Delta\dot{h}_3(t) = -\frac{a_3}{A_3}\sqrt{\frac{g}{2h_3^0}}\Delta h_3(t) + \frac{(1-\gamma_2)}{A_3}\Delta q_2(t) + \frac{1}{A_3}\Delta q_3(t)$$
$$\Delta\dot{h}_4(t) = -\frac{a_4}{A_4}\sqrt{\frac{g}{2h_4^0}}\Delta h_4(t) + \frac{(1-\gamma_1)}{A_4}\Delta q_1(t) + \frac{1}{A_4}\Delta q_4(t) \quad (60)$$

Equations (60) can be rewritten into a more suitable form by introducing relative (dimensionless) values with respect to the operating point as

$$\varphi_\chi(t) = \frac{\Delta\chi(t)}{\chi^0} \quad \rightarrow \quad \Delta\chi(t) = \varphi_\chi(t)\cdot\chi^0 \quad (61)$$

giving rise to (62) where time constants read $T_i = \frac{A_i}{a_i}\sqrt{\frac{2h_i^0}{g}}$, $i \in \{1,2,3,4\}$.

$$\dot{\varphi}_{h_1}(t) = -\frac{1}{T_1}\varphi_{h_1}(t) + \frac{A_3}{A_1}\frac{h_3^0}{h_1^0}\frac{1}{T_3}\varphi_{h_3}(t) + \frac{\gamma_1}{A_1}\frac{q_1^0}{h_1^0}\varphi_{q_1}(t)$$
$$\dot{\varphi}_{h_2}(t) = -\frac{1}{T_2}\varphi_{h_2}(t) + \frac{A_4}{A_2}\frac{h_4^0}{h_2^0}\frac{1}{T_4}\varphi_{h_4}(t) + \frac{\gamma_2}{A_2}\frac{q_2^0}{h_2^0}\varphi_{q_2}(t)$$
$$\dot{\varphi}_{h_3}(t) = -\frac{1}{T_3}\varphi_{h_3}(t) + \frac{(1-\gamma_2)}{A_3}\frac{q_2^0}{h_3^0}\varphi_{q_2}(t) + \frac{1}{A_3}\frac{q_3^0}{h_3^0}\varphi_{q_3}(t)$$
$$\dot{\varphi}_{h_4}(t) = -\frac{1}{T_4}\varphi_{h_4}(t) + \frac{(1-\gamma_1)}{A_4}\frac{q_1^0}{h_4^0}\varphi_{q_1}(t) + \frac{1}{A_4}\frac{q_4^0}{h_4^0}\varphi_{q_4}(t) \quad (62)$$

The state-space (matrix) form of (62) is

$$\begin{bmatrix}\dot{\varphi}_{h_1}(t)\\ \dot{\varphi}_{h_2}(t)\\ \dot{\varphi}_{h_3}(t)\\ \dot{\varphi}_{h_4}(t)\end{bmatrix} = \begin{bmatrix} -\frac{1}{T_1} & 0 & \frac{A_3}{A_1}\frac{h_3^0}{h_1^0}\frac{1}{T_3} & 0\\ 0 & -\frac{1}{T_2} & 0 & \frac{A_4}{A_2}\frac{h_4^0}{h_2^0}\frac{1}{T_4}\\ 0 & 0 & -\frac{1}{T_3} & 0\\ 0 & 0 & 0 & -\frac{1}{T_4}\end{bmatrix} \times \begin{bmatrix}\varphi_{h_1}(t)\\ \varphi_{h_2}(t)\\ \varphi_{h_3}(t)\\ \varphi_{h_4}(t)\end{bmatrix} + \begin{bmatrix} \frac{\gamma_1 q_1^0}{A_1 h_1^0} & 0\\ 0 & \frac{\gamma_2 q_2^0}{A_2 h_2^0}\\ 0 & \frac{(1-\gamma_2)q_2^0}{A_3 h_3^0}\\ \frac{(1-\gamma_1)q_1^0}{A_4 h_4^0} & 0\end{bmatrix} \times \begin{bmatrix}\varphi_{q_1}(t)\\ \varphi_{q_2}(t)\end{bmatrix} + \begin{bmatrix} 0 & 0\\ 0 & 0\\ \frac{q_3^0}{A_3 h_3^0} & 0\\ 0 & \frac{q_4^0}{A_4 h_4^0}\end{bmatrix} \begin{bmatrix}\varphi_{q_3}(t)\\ \varphi_{q_4}(t)\end{bmatrix}$$

TABLE 2. The values of nominal parameters in two operating points.

Operational parameters	P_1	P_2
(h_1^0, h_2^0) [cm]	(10.73, 11.87)	(10.73, 11.87)
(h_3^0, h_4^0) [cm]	(1.54, 1.51)	(4.54, 5.46)
(q_1^0, q_2^0) [cm^3·s^{-1}]	(8.0, 8.0)	(8.0, 8.0)
(q_3^0, q_4^0) [cm^3·s^{-1}]	(1.5, 1.5)	(1.5, 1.5)
(γ_1, γ_2) [-]	(0.8, 0.7)	(0.45, 0.35)

$$\begin{bmatrix}\varphi_{h_1}(t)\\ \varphi_{h_2}(t)\end{bmatrix} = \begin{bmatrix}1 & 0 & 0 & 0\\ 0 & 1 & 0 & 0\end{bmatrix} \times [\,\varphi_{h_1}(t) \;\; \varphi_{h_2}(t) \;\; \varphi_{h_3}(t) \;\; \varphi_{h_4}(t)\,]^T \quad (63)$$

where $\varphi_{h_1}(t)$ to $\varphi_{h_4}(t)$ are state variables, $\varphi_{h_1}(t) = y_1(t)$, $\varphi_{h_2}(t) = y_2(t)$ represent outputs, $\varphi_{q_1}(t) = u_1(t)$, $\varphi_{q_2}(t) = u_2(t)$ are manipulated variables (i.e., inputs) and $\varphi_{q_3}(t) = v_3(t)$, $\varphi_{q_4}(t) = v_4(t)$ stand for measurable disturbances.

By applying the Laplace transform to (63) and taking relation (57) into account, one can obtain transfer function matrices $\boldsymbol{G}_S(s)$ and $\boldsymbol{G}_{SV}(s)$ in the following forms

$$\boldsymbol{G}_S(s) = \begin{bmatrix} \frac{\gamma_1 q_1^0 c_1}{T_1 s+1} & \frac{(1-\gamma_2)\,q_2^0 c_1}{(T_1 s+1)(T_3 s+1)}\\ \frac{(1-\gamma_1)\,q_1^0 c_2}{(T_2 s+1)(T_4 s+1)} & \frac{\gamma_2 q_2^0 c_2}{T_2 s+1}\end{bmatrix} \quad (64)$$

$$\boldsymbol{G}_{SV}(s) = \begin{bmatrix} \frac{q_3^0 c_1}{(T_1 s+1)(T_3 s+1)} & 0\\ 0 & \frac{q_4^0 c_2}{(T_2 s+1)(T_4 s+1)}\end{bmatrix} \quad (65)$$

where $c_i = \frac{T_i}{A_i h_i^0}$, $i = 1, 2$.

3) NOMINAL MODELS AT OPERATING POINTS

Two distinct settings of parameters γ_1 and γ_2 are considered, giving rise to two corresponding operating points P_1 and P_2 provided to the reader in Table 2.

If $1 < \gamma_1 + \gamma_2 < 2$, then a minimum phase MIMO controlled plant (64) is obtained; whereas, whenever $0 < \gamma_1 + \gamma_2 < 1$, then the plant is non-minimum phase, i.e., at least one root of the numerator of $\det(\boldsymbol{G}_S(s))$ lies in the RHP [13], [58], [105], [106]. Illustration of computation zeros of MIMO controlled plants can be found, e.g., in [105], [106]. On the other hand, some authors understand the notion of non-minimum phase systems differently [60].

The following transfer function matrices for the two chosen operating points P_1 and P_2 can be determined

$$\boldsymbol{G}_S^{P_1}(s) = \begin{bmatrix} \frac{1.2429}{58.32s+1} & \frac{0.4660}{(58.32s+1)(22.08s+1)}\\ \frac{0.3678}{(87.35s+1)(31.12s+1)} & \frac{1.2874}{87.35s+1}\end{bmatrix} \quad (66)$$

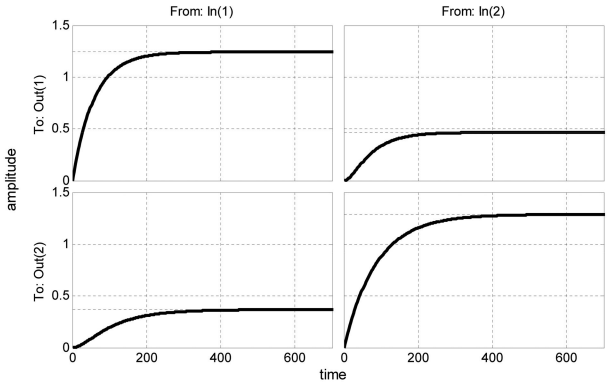

FIGURE 6. Step response of the controlled plant transfer function matrix (66).

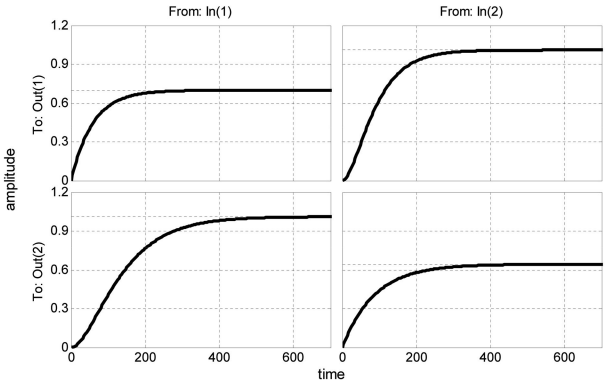

FIGURE 7. Step response of the controlled plant transfer function matrix (68).

$$\boldsymbol{G}_{SV}^{P_1}(s) = \begin{bmatrix} \dfrac{0.2913}{(58.32s+1)\,(22.08\,s+1)} & 0 \\ 0 & \dfrac{0.3448}{(87.35s+1)\,(31.12s+1)} \end{bmatrix} \tag{67}$$

$$\boldsymbol{G}_{S}^{P_2}(s) = \begin{bmatrix} \dfrac{0.6990}{58.32s+1} & \dfrac{1.0097}{(58.32s+1)\,(37.94\,s+1)} \\ \dfrac{1.0115}{(87.35s+1)\,(59.24s+1)} & \dfrac{0.6437}{87.35s+1} \end{bmatrix} \tag{68}$$

$$\boldsymbol{G}_{SV}^{P_2}(s) = \begin{bmatrix} \dfrac{0.2913}{(58.32s+1)\,(37.94\,s+1)} & 0 \\ 0 & \dfrac{0.3448}{(87.35s+1)\,(59.24s+1)} \end{bmatrix} \tag{69}$$

Step responses of $\boldsymbol{G}_{S}^{P_1}(s)$, $\boldsymbol{G}_{S}^{P_2}(s)$ (66), (68) and those of $\boldsymbol{G}_{SV}^{P_1}(s)$, $\boldsymbol{G}_{SV}^{P_2}(s)$ (67), (69) are displayed in Figs. 6 to 9.

As mentioned above, it is possible to determine whether the MIMO controlled plant $\boldsymbol{G}_S(s)$ - for the chosen operating points P_1 (66) and P_2 (68) - is minimum phase or non-minimum phase by calculating zeros of the numerator of $\det(\boldsymbol{G}_S(s))$. Thus, for the chosen operating point P_1, the roots are -0.0528, -0.0246, i.e., the MIMO controlled plant $\boldsymbol{G}_S(s)$ (66) is minimum phase. In the contrary, for the selected operating point P_2, the zeros are -0.0538, $+0.0105$, i.e., the plant (68) is non-minimum phase.

The comparison of responses of the original (nonlinear) and linearized plant models $\boldsymbol{G}_S(s)$ in the chosen operating points P_1 and P_2 are shown in Figs. 10 and 11. In Fig. 10, the input signal vector is $\boldsymbol{u}(t) = [0.15,\ 0.15]^{\mathrm{T}}$ while the disturbances are set to zero. It is apparent that the responses of y_1, y_2 for the operating point P_2 do not correspond to the typical non-minimum phase behavior. In fact, a response of a MIMO controlled plant depends on both the size and the direction of the input signal vector $\boldsymbol{u}(t) = [u_1, u_2]^{\mathrm{T}}$.

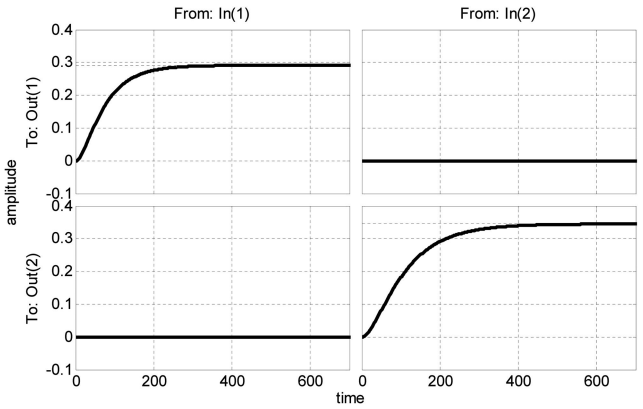

FIGURE 8. Step response of the measurable disturbance variables transfer function matrix (67).

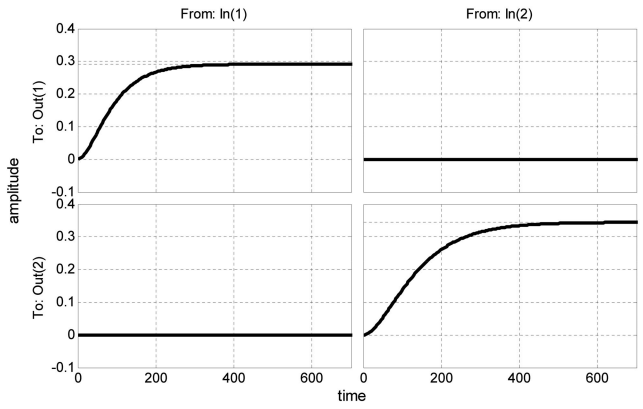

FIGURE 9. Step response of the measurable disturbance variables transfer function matrix (69).

It can be deduced from the figures that errors of the output signal responses $y_1(t)$, $y_2(t)$ (i.e., $\varphi_{h_1}(t)$, $\varphi_{h_2}(t)$), of the nonlinear vs. the linearized mathematical model vary from -2% to $+6\%$ in their steady states, for the chosen step changes of the manipulated inputs and disturbances.

On the contrary, $\boldsymbol{u}(t) = [-0.1,\ 0.1]^{\mathrm{T}}$ in Fig. 11 and both the outputs for the operating point P_2 show a typical non-minimum phase behavior.

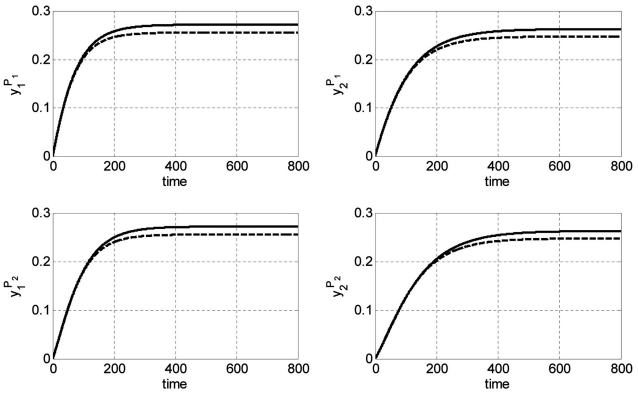

FIGURE 10. Comparison of nonlinear (solid line) and linearized mathematical model (dashed line) responses related to operating points P_1 (top) and P_2 (bottom) for input signals $u_1 = u_2 = 0.15$ (i.e., $\Delta q_1 = \Delta q_2 = 1.2\ \text{cm}^3 \cdot \text{s}^{-1}$) and $v_1 = v_2 = 0$.

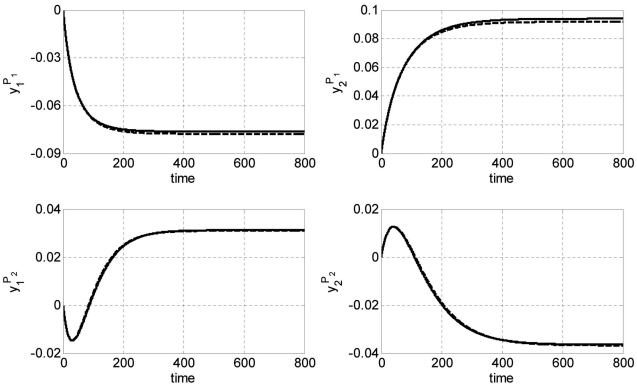

FIGURE 11. Comparison of nonlinear (solid line) and linearized mathematical model (dashed line) responses related to operating points P_1 (top) and P_2 (bottom) for input signals $u_1 = -0.1$, $u_2 = 0.1$ (i.e., $\Delta q_1 = -0.8$, $\Delta q_2 = 0.8\ \text{cm}^3 \cdot \text{s}^{-1}$) and $v_1 = v_2 = 0$.

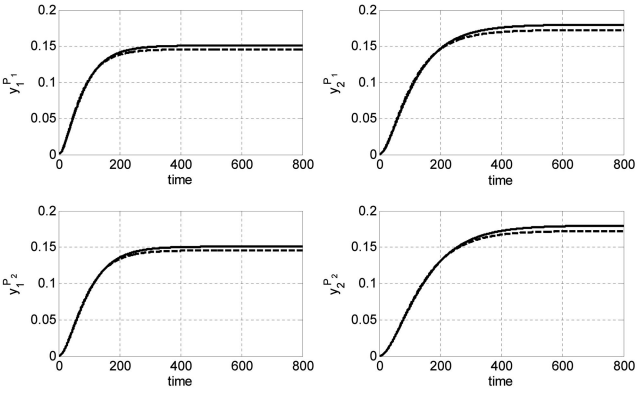

FIGURE 12. Comparison of nonlinear (solid line) and linearized mathematical model (dashed line) responses related to operating points P_1 (top) and P_2 (bottom) for input signals $u_1 = u_2 = 0$ and $v_1 = v_2 = 0.5$ (i.e., $\Delta q_3 = \Delta q_4 = 0.75\ \text{cm}^3 \cdot \text{s}^{-1}$).

In Fig. 12, output responses for P_1 and P_2 are displayed when the manipulated inputs are set to zero, while the vector of input disturbances reads $\boldsymbol{v}(t) = [0.5, 0.5]^{\mathrm{T}}$.

B. SYNTHESIS OF THE TWO-VARIABLE CONTROL LOOP FOR THE QUADRUPLE-TANK PROCESS

The control design procedure summarized in Subsection II.E is applied to the two-variable control system of the quadruple-tank process.

1) OPTIMAL CONTROL PAIRS DETERMINATION

Tools and techniques introduced in Subsection II.B are used now to determine the optimal control pairs for the controlled plant transfer function matrices $\boldsymbol{G}_S^{P_1}(s)$ (66) and $\boldsymbol{G}_S^{P_2}(s)$ (68). The eventual results are as follows.

1) RGA (10):

$$\boldsymbol{\Lambda}_0^{P_1} = \boldsymbol{K}^{P_1} \otimes \left(\boldsymbol{K}^{P_1}\right)^{-T} = \begin{bmatrix} 1.120 & -0.120 \\ -0.120 & 1.120 \end{bmatrix}$$
$$\boldsymbol{\Lambda}_0^{P_2} = \boldsymbol{K}^{P_2} \otimes \left(\boldsymbol{K}^{P_2}\right)^{-T} = \begin{bmatrix} -0.788 & 1.788 \\ 1.7885 & -0.788 \end{bmatrix} \tag{70}$$

where

$$\boldsymbol{K}^{P_1} = \boldsymbol{G}_S^{P_1}(0) = \begin{bmatrix} 1.243 & 0.466 \\ 0.368 & 1.287 \end{bmatrix},$$
$$\boldsymbol{K}^{P_2} = \boldsymbol{G}_S^{P_2}(0) = \begin{bmatrix} 0.699 & 1.010 \\ 1.012 & 0.644 \end{bmatrix}$$

2) RNGA (16)–(18):

$$\boldsymbol{\Lambda}_{N,0}^{P_1} = \boldsymbol{K}_N^{P_1} \otimes \left(\boldsymbol{K}_N^{P_1}\right)^{-T} = \begin{bmatrix} 1.061 & -0.061 \\ -0.061 & 1.061 \end{bmatrix}$$
$$\boldsymbol{\Lambda}_{N,0}^{P_2} = \boldsymbol{K}_N^{P_2} \otimes \left(\boldsymbol{K}_N^{P_2}\right)^{-T} = \begin{bmatrix} 5.539 & -4.539 \\ -4.539 & 5.539 \end{bmatrix} \tag{71}$$

where

$$\boldsymbol{K}_N^{P_1} = \boldsymbol{G}_S^{P_1}(0) \odot \boldsymbol{T}_{AR}^{P_1} = \begin{bmatrix} 0.0213 & 0.0058 \\ 0.0031 & 0.0147 \end{bmatrix},$$
$$\boldsymbol{K}_N^{P_2} = \boldsymbol{G}_S^{P_2}(0) \odot \boldsymbol{T}_{AR}^{P_2} = \begin{bmatrix} 0.0120 & 0.0105 \\ 0.0069 & 0.0074 \end{bmatrix},$$
$$\boldsymbol{T}_{AR}^{P_1} = \begin{bmatrix} 58.32 & 80.40 \\ 118.47 & 87.35 \end{bmatrix},$$
$$\boldsymbol{T}_{AR}^{P_2} = \begin{bmatrix} 58.32 & 96.26 \\ 146.59 & 87.35 \end{bmatrix}$$

3) CN (23), (24):

$$CN_1^{P_1} = \frac{\sigma_{\max}\left(\boldsymbol{K}^{P_1}\right)}{\sigma_{\min}\left(\boldsymbol{K}^{P_1}\right)} = 1.984,$$
$$CN_2^{P_1} = \frac{\sigma_{\max}\left(\boldsymbol{K}_N^{P_1}\right)}{\sigma_{\min}\left(\boldsymbol{K}_N^{P_1}\right)} = 1.882$$
$$CN_1^{P_2} = \frac{\sigma_{\max}\left(\boldsymbol{K}^{P_2}\right)}{\sigma_{\min}\left(\boldsymbol{K}^{P_2}\right)} = 4.954,$$
$$CN_2^{P_2} = \frac{\sigma_{\max}\left(\boldsymbol{K}_N^{P_2}\right)}{\sigma_{\min}\left(\boldsymbol{K}_N^{P_2}\right)} = 22.255 \tag{72}$$

a: OPERATING POINT P_1

Regarding result (72) for operating point P_1, condition numbers $CN_1^{P_1} < 10$ (for $\boldsymbol{K}$) and $CN_2^{P_1} < 10$ (for $\boldsymbol{K}_N$) indicate that the controlled plant can be decoupled; i.e., it is possible to determine the optimal control pairs. These optimal pairs are y_1-u_1 (i.e., $\varphi_{h_1} - \varphi_{q_1}$) and y_2-u_2 (i.e., $\varphi_{h_2} - \varphi_{q_2}$), according to (70) and (71), and they correspond to transfer functions (i.e., dominant elements of $\boldsymbol{G}_S^{P_1}(s)$ (66)) $S_{11}^{P_1}$ and $S_{22}^{P_1}$. Then, by following (30), one can denote $\tilde{S}_{11}^{P_1} = S_{11}^{P_1}$, $\tilde{S}_{22}^{P_1} = S_{22}^{P_1}$.

The stability of the resulting control structure, i.e., the control loop that uses determined optimal control pairs, can be verified by using the NI value (22). The eventual values given in (73) indicates (for P_1) that the determined control pairs y_1-u_1 and y_2-u_2 should yield the stability of the feedback control loop.

$$\begin{aligned} NI^{P_1} &= \frac{\det\left(\boldsymbol{G}_S^{P_1}(0)\right)}{\prod_{i=1}^{n} S_{ii}^{P_1}(0)} = \frac{\det\left(\boldsymbol{K}^{P_1}\right)}{\prod_{i=1}^{n} k_{ii}^{P_1}} \\ &= \frac{\det\begin{bmatrix} 1.120 & -0.120 \\ -0.120 & 1.120 \end{bmatrix}}{1.120 \cdot 1.120} = \frac{1.240}{1.254} \\ &= 0.989 > 0 \end{aligned} \tag{73}$$

b: OPERATING POINT P_2

Values of CN for P_2 provided to the reader in (72) indicate that the MIMO controlled plant can be decoupled when using the RGA tool ($CN_1^{P_2} < 10$); however, condition number $CN_2^{P_2} > 10$ resulting from the RNGA yields that the MIMO controlled plant might be ill-conditioned and, hence, difficult to be controlled, which has also been verified by simulation experiments. Therefore, eventual optimal control pairs are determined based on only the RGA tool but not the RNGA one. Then, result (71) gives rise to the dominant pairing y_1-u_2 and y_2-u_1 with the corresponding transfer functions $S_{12}^{P_2}$ and $S_{21}^{P_2}$, respectively, i.e., $\tilde{S}_{12}^{P_2} = S_{12}^{P_2}$, $\tilde{S}_{12}^{P_2} = S_{12}^{P_2}$, see (30). The NI value (22) is

$$\begin{aligned} NI^{P_2} &= \frac{\det\left(\boldsymbol{G}_S^{P_2}(0)\right)}{\prod_{i=1}^{n} S_{ii}^{P_2}(0)} = \frac{\det\left(\boldsymbol{K}^{P_2}\right)}{\prod_{i=1}^{n} k_{ii}^{P_2}} \\ &= \frac{\det\begin{bmatrix} 1.788 & -0.788 \\ -0.788 & 1.788 \end{bmatrix}}{1.788 \cdot 1.788} = \frac{2.575}{3.195} \\ &= 0.388 > 0 \end{aligned} \tag{74}$$

which implies that the determined control pairs y_1-u_2 and y_2-u_1 should ensure the stability of the control loop.

Optimal disturbance control pairs y_i-v_j for operating points P_1 and P_2 can be determined using the transfer function matrices $\boldsymbol{G}_{SV}^{P_1}(s)$ (67) and $\boldsymbol{G}_{SV}^{P_2}(s)$ (69). In these cases, it is obvious that optimal control pairs for operating points P_1 and P_2 are y_1-v_1 (i.e., $\varphi_{h_1} - \varphi_{q_3}$) and y_2-v_2 ($\varphi_{h_2} - \varphi_{q_4}$). The corresponding transfer functions $S_{V,11}^{P_1}$ and $S_{V,22}^{P_1}$ represent dominant entries of $\boldsymbol{G}_{SV}^{P_1}(s)$ for P_1, i.e. $\tilde{S}_{V,11}^{P_1} = S_{V,11}^{P_1}$, $\tilde{S}_{V,22}^{P_1} = S_{V,22}^{P_1}$. For operating point P_2, one gets corresponding transfer functions $\tilde{S}_{V,11}^{P_2} = S_{V,11}^{P_2}$ and $\tilde{S}_{V,22}^{P_2} = S_{V,22}^{P_2}$.

2) PARAMETERS DETERMINATION FOR AUXILIARY CONTROLLERS, PRIMARY CONTROLLERS, AND CORRECTION MEMBERS

a: OPERATING POINT P_1

Auxiliary controllers RP^{P_1} for operating point P_1 are determined by using (30). Recall that the dominant elements of $\boldsymbol{G}_S^{P_1}(s)$ have been determined as $\tilde{S}_{11}^{P_1}, \tilde{S}_{22}^{P_1}$ (see Subsection III.B.1), whereas the remaining elements are non-dominant. Then, transfer function matrix of the auxiliary controllers $\boldsymbol{G}_{RP}^{P_1}(s)$ is gained in the form

$$\begin{aligned} \boldsymbol{G}_{RP}^{P_1}(s) &= \begin{bmatrix} 0 & RP_{12}^{P_1} \\ RP_{21}^{P_1} & 0 \end{bmatrix} \\ RP_{12}^{P_1} &= \frac{S_{12}^{P_1}}{\tilde{S}_{11}^{P_1}} = \frac{0.0170}{s + 0.0453} \\ RP_{21}^{P_1} &= \frac{S_{21}^{P_1}}{\tilde{S}_{22}^{P_1}} = \frac{0.00918}{s + 0.0321} \end{aligned} \tag{75}$$

As indicated in Section I, we intend provide the reader with a rich comparative study to demonstrate the performance of the proposed method. First, the reason for using the optimal control pairs is demonstrated by the comparison with the non-optimal (i.e., the off-diagonal) pairing. Since (30) yields non-feasible controllers, in this case, the following low-pass filter with the time constant T_F, in accordance with (35), is used

$$C_{12} = C_{21} = \frac{1}{T_F s + 1} \tag{76}$$

Let us set $T_F = 1$, which gives rise to

$$\boldsymbol{G}_{RP}^{P_1}(s) = \begin{bmatrix} 0 & \dfrac{108.9s + 3.5}{s + 1} \\ \dfrac{58.89s + 2.667}{s + 1} & 0 \end{bmatrix} \tag{77}$$

Intuitively, a higher value of T_F in (76) should result in a slower response (since the open-loop dynamics is affected more significantly) yet it improves the feasibility. To verify this issue, let us select $T_F = 10$ in addition, which yields

$$\boldsymbol{G}_{RP}^{P_1}(s) = \begin{bmatrix} 0 & \dfrac{108.9s + 3.5}{10s + 1} \\ \dfrac{58.89s + 2.667}{10s + 1} & 0 \end{bmatrix} \tag{78}$$

In addition, a simplified decoupler [45], [60], the standard inverted decoupler [56], an inverted fuzzy decoupler [73], a centralized inverted PI(D) decoupling control [64], [58], and a polynomial centralized coupled approach [92], [93] are considered for the comparisons. The fuzzy decoupler is characterized by fuzzy rules that cannot be expressed by transfer functions. Due to Remark 3, the standard inverted decoupler agrees with (75). The centralized inverted PI(D) decoupling control does not include the explicit decoupler but

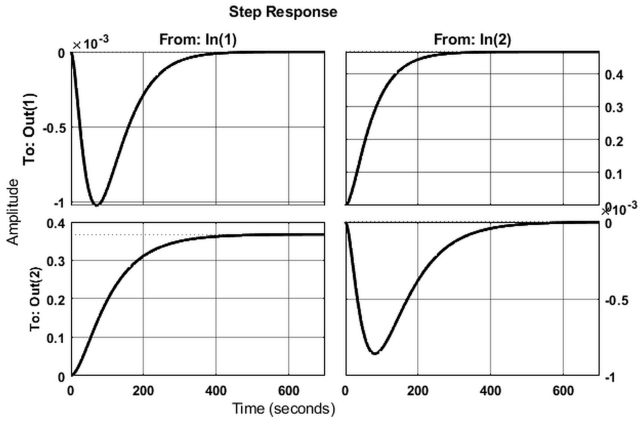

FIGURE 13. Step response of the open-loop transfer function matrix $\boldsymbol{H}(s)$ with (66) and (77).

the primary controller itself should ensure this feature. The polynomial approach does not intend to decouple the control loops. Finally, the simplified decoupler results in

$$\boldsymbol{G}_{RP}^{P_1}(s) = \begin{bmatrix} 1 & \dfrac{-0.3749}{22.0799s+1} \\ \dfrac{0.2857}{31.1236s+1} & 1 \end{bmatrix} \tag{79}$$

Regarding primary controllers, the proposed optimal pairings with auxiliary controller transfer function matrix (75) give the ideal decoupling according to (28). The use of rule (49) empowers $R_{11}^{P_1}$ and $R_{22}^{P_1}$ (corresponding to $S_{11}^{P_1}$ and $S_{22}^{P_1}$, respectively) as the primary controllers for $\boldsymbol{G}_S^{P_1}(s)$. These SISO controllers are to be appropriately tuned. The MOM [89], [97] is herein used for integral controllers and the BTM [94]–[96] for proportional-integral (PI) controllers. These methods give rise to the eventual controller transfer functions.

1) MOM:

$$\boldsymbol{G}_R^{P_1}(s) = \begin{bmatrix} \dfrac{1}{144.918\,s} & 0 \\ 0 & \dfrac{1}{224.909\,s} \end{bmatrix} \tag{80}$$

2) BTM:

$$\boldsymbol{G}_R^{P_1}(s) = \begin{bmatrix} \dfrac{0.8046s+0.0138}{s} & 0 \\ 0 & \dfrac{0.7768s+0.00889}{s} \end{bmatrix} \tag{81}$$

Note that besides the above-mentioned methods, other SISO synthesis methods can be used by the reader.

The use of $\boldsymbol{G}_{RP}^{P_1}(s)$ as in (77) and (78) for the non-optimal pairs results in a non-ideal decoupling. However, the loops are decoupled asymptotically. It can be seen from the step response of the open-loop transfer function matrix $\boldsymbol{H}(s)$ which is displayed in Fig. 13; i.e., the diagonal elements are non-zero, except for the zero frequency.

Then, primary controllers (82) and (83) can be obtained by using (48), (49) and by the BTM tuning rules for $T_F = 1$ and $T_F = 10$, respectively.

$$\boldsymbol{G}_R^{P_1}(s) = \begin{bmatrix} 0 & \dfrac{1.745s+0.02588}{s} \\ \dfrac{2.224s+0.02223}{s} & 0 \end{bmatrix} \tag{82}$$

$$\boldsymbol{G}_R^{P_1}(s) = \begin{bmatrix} 0 & \dfrac{1.361s+0.01772}{s} \\ \dfrac{1.663s+0.01537}{s} & 0 \end{bmatrix} \tag{83}$$

When using the fuzzy decoupler, the primary controller (81) is used.

For the simplified decoupler (79), the BTM technique gives

$$\boldsymbol{G}_R^{P_1}(s) = \begin{bmatrix} \dfrac{0.9011s+0.01744}{s} & 0 \\ 0 & \dfrac{0.8699s+0.01071}{s} \end{bmatrix} \tag{84}$$

Note that even if no loop interactions appear for (79), relation (28) cannot be used since the open-loop transfer function matrix does not equal to $\boldsymbol{G}_S^{P_1}(s)$. Hence, controllers (84) have to be calculated based on (48).

The centralized inverted decoupling control design yields the primary controller matrix

$$\boldsymbol{G}_R^{P_1}(s) = \begin{bmatrix} \dfrac{0.780s+0.01502}{s} & \dfrac{-0.3201s-0.005436}{s} \\ \dfrac{-0.08932s-0.004291}{s} & \dfrac{1.174s+0.0145}{s} \end{bmatrix} \tag{85}$$

where the gain stability margins are set to $A_{m1} = A_{m2} = 3$ for the critical frequencies $\omega_{c1} = \omega_{c2} = 0.05\,\mathrm{rad}\cdot\mathrm{s}^{-1}$, see further details, e.g. in [58].

Finally, the centralized polynomial approach results in

$$\boldsymbol{G}_R^{P_1}(s) = \begin{bmatrix} R_{11}^{P_1} & R_{12}^{P_1} \\ R_{21}^{P_1} & R_{22}^{P_1} \end{bmatrix}$$

$$R_{11}^{P_1} = \frac{0.568s^3 + 0.05372s^2 + 0.001581s + 1.417\cdot 10^{-5}}{s^3 + 0.0732s^2 + 0.001282s}$$

$$R_{12}^{P_1} = \frac{-1.067s^3 - 0.08863s^2 - 0.002229s - 1.551\cdot 10^{-5}}{s^3 + 0.0732s^2 + 0.001282s}$$

$$R_{21}^{P_1} = \frac{-0.0923s^3 - 0.01203s^2 - 0.0004632s - 4.87\cdot 10^{-6}}{s^3 + 0.0732s^2 + 0.001282s}$$

$$R_{22}^{P_1} = \frac{1.406s^3 + 0.1249s^2 + 0.003291s + 2.342\cdot 10^{-5}}{s^3 + 0.0732s^2 + 0.001282s} \tag{86}$$

where the closed-loop poles are set equal to the poles of the controlled plant model (66). Notice that PI controllers are no longer possible to be obtained here.

Correction members KC^{P_1} are determined by using (50), (51) (for absolute invariance) and (52) (for approximate invariance). For the former case, one gets

$$\boldsymbol{G}_{KC}^{P_1}(s) = \begin{bmatrix} \dfrac{0.0106s + 0.000341}{s^2 + 0.0774s + 0.0013} & \dfrac{-0.000146}{s^2 + 0.0774s + 0.0013} \\ \dfrac{-9.743 \cdot 10^{-5}}{s^2 + 0.0774s + 0.0013} & \dfrac{0.00861s + 0.000390}{s^2 + 0.0774s + 0.0013} \end{bmatrix} \tag{87}$$

Regarding the latter case, dominant elements of $\boldsymbol{G}_{SV}^{P_1}(s)$ (67) are determined as $\tilde{S}_{V,11}^{P_1}, \tilde{S}_{V,22}^{P_1}$. Thus, correction members KC^{P_1} ensuring approximate invariance have forms

$$\begin{aligned} \boldsymbol{G}_{KC}^{P_1}(s) &= \begin{bmatrix} KC_{11}^{P_1} & 0 \\ 0 & KC_{22}^{P_1} \end{bmatrix} \\ KC_{11}^{P_1} &= \frac{\tilde{S}_{V,11}^{P_1}}{\tilde{S}_{11}^{P_1}} = \frac{S_{V,11}^{P_1}}{S_{11}^{P_1}} = \frac{0.0106}{s + 0.0453} \\ KC_{22}^{P_1} &= \frac{\tilde{S}_{V,22}^{P_1}}{\tilde{S}_{22}^{P_1}} = \frac{S_{V,22}^{P_1}}{S_{22}^{P_1}} = \frac{0.00861}{s + 0.0321} \end{aligned} \tag{88}$$

b: OPERATING POINT P_2

The use of (30) for the operating point P_2 (governed by the non-minimum phase MIMO controlled plant $\boldsymbol{G}_S^{P_2}(s)$ (68)) results in non-feasible auxiliary controllers RP^{P_2} of negative relative degrees. Hence, there are two possibilities here. Namely, one can abandon the endeavor to cancel interactions between control loops or to utilize the compensator (35). Assume the following two options: Either the low-pass filter is as in (76) or

$$C_{12} = \frac{1}{T_F s + 1}, \quad C_{21} = -C_{12} \tag{89}$$

When using (76), it was observed by simulations that low values of $T_F \approx (0, 30]$ result in unstable open-loop $\boldsymbol{H}(s)$, high values $T_F > 55$ yield a periodic control response. We eventually set $T_F = 35$ giving rise to

$$\boldsymbol{G}_{RP}^{P_2}(s) = \begin{bmatrix} 0 & \dfrac{37.7s + 0.6364}{35s + 1} \\ \dfrac{26.26s + 0.6923}{35s + 1} & 0 \end{bmatrix} \tag{90}$$

In this case, the open-loop model $\boldsymbol{H}(s)$ is not ideally yet asymptotically decoupled, as clear from its step response displayed in Fig. 14.

If compensator (89) is applied, low values of $T_F \approx (0, 5]$ give very slow control responses. On the other hand, high values $T_F > 30$ produce controlled output oscillations as well. The chosen setting $T_F = 10$ then yields the decoupler

$$\boldsymbol{G}_{RP}^{P_2}(s) = \begin{bmatrix} 0 & \dfrac{37.7s + 0.6364}{10s + 1} \\ -\dfrac{26.26s + 0.6923}{10s + 1} & 0 \end{bmatrix} \tag{91}$$

It is worth noting that $\boldsymbol{H}(s)$ with (91) is not decoupled, even for the zero frequency (see Fig. 15).

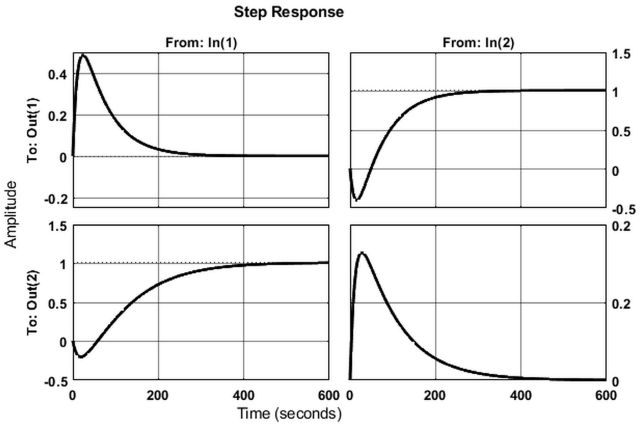

FIGURE 14. Step response of the open-loop transfer function matrix $\boldsymbol{H}(s)$ with (68) and (90).

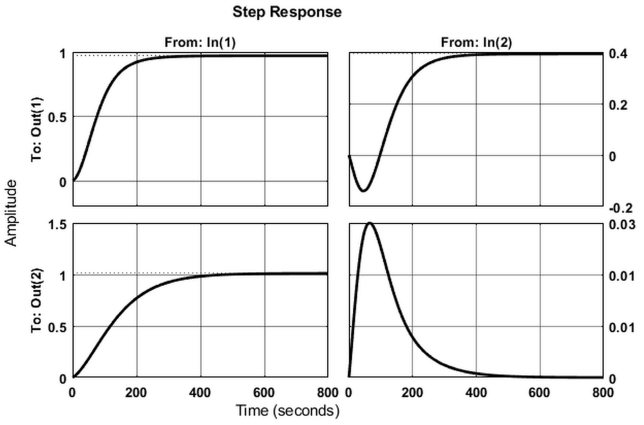

FIGURE 15. Step response of the open-loop transfer function matrix $\boldsymbol{H}(s)$ with (68) and (91).

The standard inverted decoupler according to Proposition 1 (43) and (41) reads

$$\bar{\boldsymbol{G}}_{RP}^{P_2}(s) = \begin{bmatrix} -1 & \dfrac{1.4445}{37.94\,s + 1} \\ \dfrac{1.571}{59.24s + 1} & -1 \end{bmatrix} \tag{92}$$

The simplified decoupler is

$$\boldsymbol{G}_{RP}^{P_2}(s) = \begin{bmatrix} \dfrac{-1.4446}{37.9363s + 1} & 1 \\ 1 & \dfrac{-1.5717}{59.2417s + 1} \end{bmatrix} \tag{93}$$

Recall that the remaining herein compared methods do not expose decoupler explicitly or do not attempt to break loop interactions.

Now, let us determine the controllers and correction members for operating point P_2. Optimal control pairs for $\boldsymbol{G}_S^{P_2}(s)$ are $R_{12}^{P_2}$ and $R_{21}^{P_2}$ that correspond to $S_{21}^{P_2}$ and $S_{12}^{P_2}$, respectively.

Assume initially the decoupling as if it was ideal, in accordance with (28). Then, the use of the MOM and the DMM [1] for PI controllers gives, respectively

1) MOM:

$$\boldsymbol{G}_R^{P_2}(s) = \begin{bmatrix} 0 & \dfrac{0.729s + 0.00835}{s} \\ \dfrac{0.761s + 0.0131}{s} & 0 \end{bmatrix} \tag{94}$$

2) DMM:

$$\boldsymbol{G}_R^{P_2}(s) = \begin{bmatrix} 0 & \dfrac{1.085s + 0.00935}{s} \\ \dfrac{1.256s + 0.0163}{s} & 0 \end{bmatrix} \tag{95}$$

Note that the ideal decoupling is reached when using the standard inverted decoupler in the 2-1 configuration (41) or via the proposed modified (nested) inverted decoupler (92).

If filtered decouplers (90) and (91) are applied, the primary controllers tuned by the DDM for the open-loop transfer function matrices $\boldsymbol{H}(s)$ (or, more precisely, for $\bar{\boldsymbol{H}}(s)$ given by (48)) read, respectively,

$$\boldsymbol{G}_R^{P_2}(s) = \begin{bmatrix} 0 & \dfrac{0.6443s + 0.01001}{s} \\ \dfrac{0.7964s + 0.007333}{s} & 0 \end{bmatrix} \tag{96}$$

$$\boldsymbol{G}_R^{P_2}(s) = \begin{bmatrix} 0 & \dfrac{0.7437s + 0.01027}{s} \\ \dfrac{1.182s + 0.01005}{s} & 0 \end{bmatrix} \tag{97}$$

The use of the simplified decoupler (93) by using (48), (49) gives rise to

$$\boldsymbol{G}_R^{P_2}(s) = \begin{bmatrix} 0 & \dfrac{-0.3729s - 0.003838}{s} \\ \dfrac{-0.4512s - 0.003814}{s} & 0 \end{bmatrix} \tag{98}$$

We use controller (95) for numerical comparative study in the case of using the fuzzy controller [73].

The centralized inverted PI decoupling controller [64], [58] (for the same settings as in the operating point P_1) reads

$$\boldsymbol{G}_R^{P_2}(s) = \begin{bmatrix} \dfrac{-0.1649s - 0.003947}{s} & \dfrac{0.2034s + 0.006192}{s} \\ \dfrac{-0.1084s + 0.006203}{s} & \dfrac{-0.3035s - 0.004287}{s} \end{bmatrix} \tag{99}$$

Finally, the polynomial centralized coupled controller design [92], [93] gives rise to the primary controller

$$\boldsymbol{G}_R^{P_2}(s) = \begin{bmatrix} R_{11}^{P_1} & R_{12}^{P_1} \\ R_{21}^{P_1} & R_{22}^{P_1} \end{bmatrix}$$

$$\begin{aligned} R_{11}^{P_2} &= \frac{-3.019s^3 - 0.179s^2 - 0.003699s - 2.603 \cdot 10^{-5}}{s^3 + 0.2057s^2 + 0.00772s} \\ R_{12}^{P_2} &= \frac{12.35s^3 + 1.136s^2 + 0.0247s + 1.524 \cdot 10^{-4}}{s^3 + 0.2057s^2 + 0.00772s} \\ R_{21}^{P_2} &= \frac{2.608s^3 + 0.3125s^2 + 0.009551s + 8.503 \cdot 10^{-5}}{s^3 + 0.2057s^2 + 0.00772s} \\ R_{22}^{P_2} &= \frac{-3.983s^3 - 0.1807s^2 - 0.002666s - 1.282 \cdot 10^{-5}}{s^3 + 0.2057s^2 + 0.00772s} \end{aligned} \tag{100}$$

Again, the closed-loop poles are set equal to the poles of the controlled plant model (68).

Correction members (as entries of $\boldsymbol{G}_{KC}^{P_2}(s)$) calculated by using (50), (51) for (68) and (69) to get absolute invariance are unstable. This nuisance is caused by the inversion of $\det(\boldsymbol{G}_S(s))$, as clear from (51); i.e., the RHP zeros of $\boldsymbol{G}_S^{P_2}(s)$ become the RPH poles of $\boldsymbol{G}_{KC}^{P_2}(s)$. To overcome this issue, one can use the correction term

$$C_{ij} = \frac{s - s_0}{-s - s_0}, \quad i, j \in \{1, 2\} \tag{101}$$

where $s_0 = 0.105$ is the RHP zero of $\boldsymbol{G}_S^{P_2}(s)$, in the sense of (35). Then, the modified $\boldsymbol{G}_{KC}^{P_2}(s)$ reads, (102), as shown at the bottom of the next page.

Another option is to use formula (52) to get approximate invariance of the MIMO control loop, at least. Recall that dominant elements of $\boldsymbol{G}_S^{P_2}(s)$ (68) and $\boldsymbol{G}_{SV}^{P_2}(s)$ (69) have been found as $\tilde{S}_{12}^{P_2} = S_{12}^{P_2}$, $\tilde{S}_{21}^{P_2} = S_{21}^{P_2}$ and $\tilde{S}_{V,11}^{P_2} = S_{V,11}^{P_2}$, $\tilde{S}_{V,22}^{P_2} = S_{V,22}^{P_2}$, respectively. Thus, (52) yields

$$\begin{aligned} \boldsymbol{G}_{KC}^{P_2}(s) &= \begin{bmatrix} 0 & KC_{12}^{P_2} \\ KC_{21}^{P_2} & 0 \end{bmatrix} \\ KC_{12}^{P_2} &= \frac{\tilde{S}_{V,22}^{P_2}}{\tilde{S}_{21}^{P_2}} = \frac{S_{V,22}^{P_2}}{S_{21}^{P_2}} = 0.341 \\ KC_{21}^{P_2} &= \frac{\tilde{S}_{V,11}^{P_2}}{\tilde{S}_{12}^{P_2}} = \frac{S_{V,11}^{P_2}}{S_{12}^{P_2}} = 0.289 \end{aligned} \tag{103}$$

C. SIMULATION RESULTS

Computational and simulation MATLAB/SIMULINK software is used to verify the proposed control design for the TITO control loop by simulations. In addition, selected numerical results for other benchmarked approaches are provided to the reader. The used block simulation scheme for the proposed method is shown in Fig. 16, while Fig. 17 displays its element-by-elements structure.

a: OPERATING POINT P_1

Control responses of the TITO control loop for the quadruple tank in the operating point P_1, using the proposed method and the selected SISO synthesis methods, are shown in Figs. 18 to 23.

Additional simulations are made to compare these results with those obtained by other selected methods. Namely, results for the proposed (and also the standard) decoupling

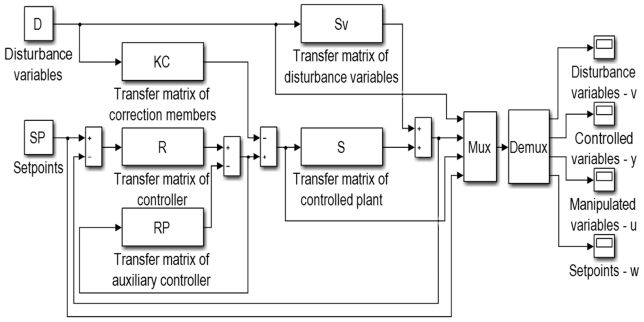

FIGURE 16. Simulation block scheme of TITO control loop created via MATLAB/SIMULINK software.

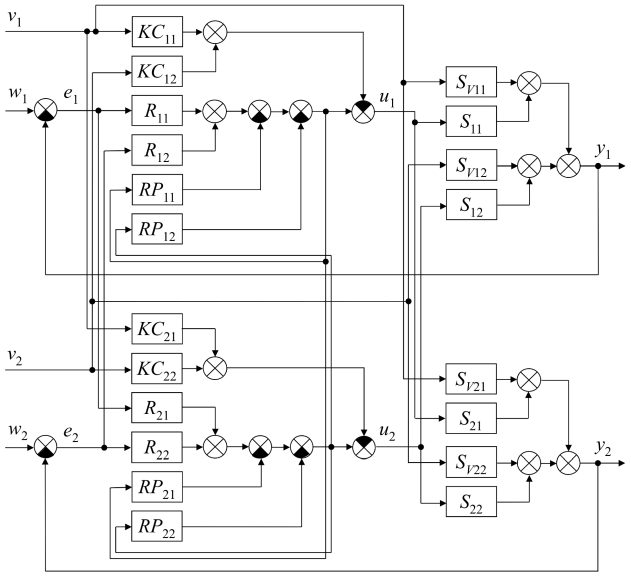

FIGURE 17. Element-by-element formulation of the general modified TITO branched control loop with disturbance variables measurement.

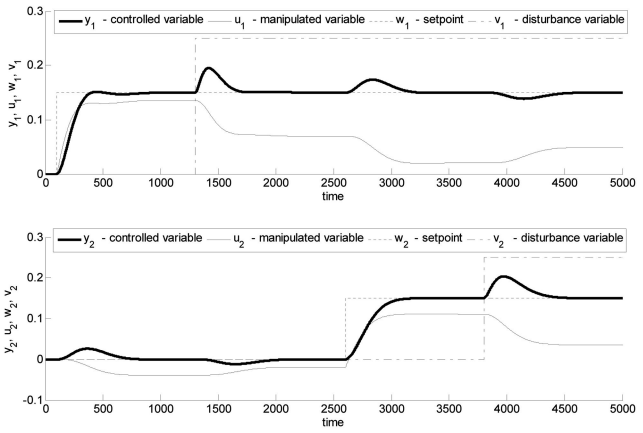

FIGURE 18. Control responses for operating point P_1 when using primary controller (80) tuned by the MOM only, i.e., without auxiliary controllers *RP* and correction members *KC*.

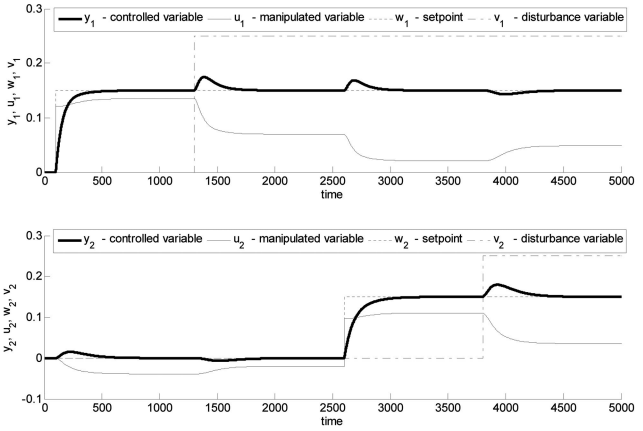

FIGURE 19. Control responses for operating point P_1 when using primary controller (81) tuned by the BTM only, i.e., without auxiliary controllers *RP* and correction members *KC*.

scheme with the non-optimal pairings governed by (77), (78), (82) and (83) are displayed in Figs. 24 and 25. Control responses when using the simplified decoupler (79) with the primary controller (84) are given in Fig. 26. The fuzzy decoupler combined with the primary controller (81) yields responses as in Fig. 27. Simulation results for the centralized inverted PI decoupling controller (85) are provided in Fig. 28. Finally, the use of the centralized polynomial approach with the primary controller transfer function matrix (86) gives responses shown in Fig. 29. Note that for all these comparative results, the ideal correction member (87) is considered.

The following parameters have been set in the figures: the time vector of step-wise setpoint changes is $[t_{w1}, t_{w2}]^{\mathrm{T}} = [100, 2600]^{\mathrm{T}}$ s with the corresponding vector of step-wise setpoints $[w_1, w_2]^{\mathrm{T}} = [0.15, 0.15]^{\mathrm{T}}$; the time vector of step-wise disturbance changes equals $[t_{v1}, t_{v2}]^{\mathrm{T}} = [1300, 3800]^{\mathrm{T}}$ s with the corresponding vector of disturbances $[v_1, v_2]^{\mathrm{T}} = [0.25, 0.25]^{\mathrm{T}}$; the time step size is $k = 0.1$ s, and the total time of simulation reads $t_s = 5000$ s.

Recall again that the corresponding notation of variables in the control-response simulations for the quadruple-tank process (see Fig. 5) are as follows: controlled variables $y_1(t) \rightarrow \varphi_{h_1}(t)$, $y_2(t) \rightarrow \varphi_{h_2}(t)$, manipulated variables $u_1(t) \rightarrow \varphi_{q_1}(t)$, $u_2(t) \rightarrow \varphi_{q_2}(t)$, reference values $w_1(t) \rightarrow \varphi_{h_1}(t)$, $w_2 \rightarrow \varphi_{h_2}(t)$, and disturbance variables $v_1(t) \rightarrow \varphi_{q_3}(t)$, $v_2(t) \rightarrow \varphi_{q_4}(t)$.

$$\boldsymbol{G}_{KC}^{P_2}(s) = \begin{bmatrix} \dfrac{-0.01098s - 1.854 \cdot 10^{-4}}{s^2 + 0.06427s + 5.651 \cdot 10^{-4}} & \dfrac{3.444 \cdot 10^{-4}}{s^2 + 0.06427s + 5.651 \cdot 10^{-4}} \\ \dfrac{2.914 \cdot 10^{-4}}{s^2 + 0.06427s + 5.651 \cdot 10^{-4}} & \dfrac{-0.09044s - 2.384 \cdot 10^{-4}}{s^2 + 0.06427s + 5.651 \cdot 10^{-4}} \end{bmatrix} \tag{102}$$

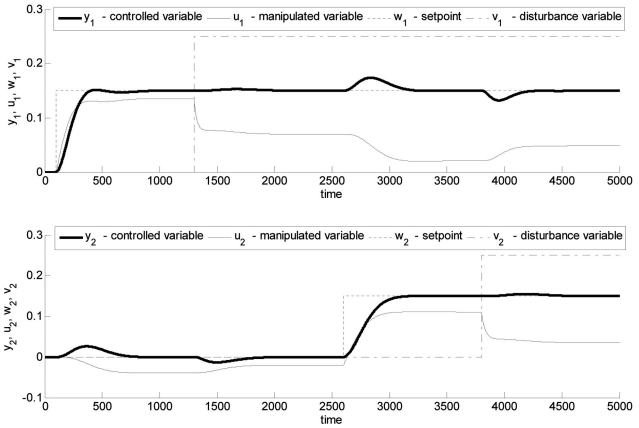

FIGURE 20. Control responses for operating point P_1 when using primary controller (80) tuned by the MOM, without auxiliary controllers *RP* yet with correction members *KC* (88) providing approximate invariance of the control loop.

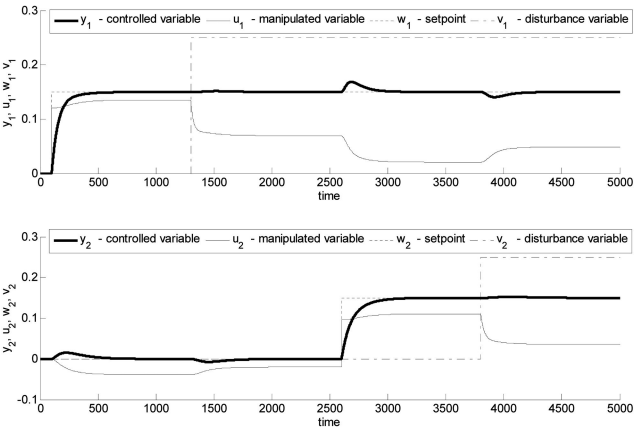

FIGURE 21. Control responses for operating point P_1 when using primary controller (81) tuned by the BTM, without auxiliary controllers *RP* yet with correction members *KC* (88) providing approximate invariance of the control loop.

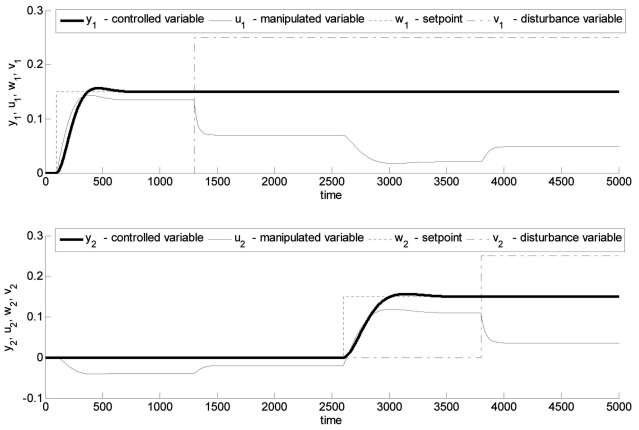

FIGURE 22. Control responses for operating point P_1 when using primary controller (80) tuned by the MOM, with auxiliary controllers *RP* (75) and correction members *KC* (87) providing absolute invariance of the control loop.

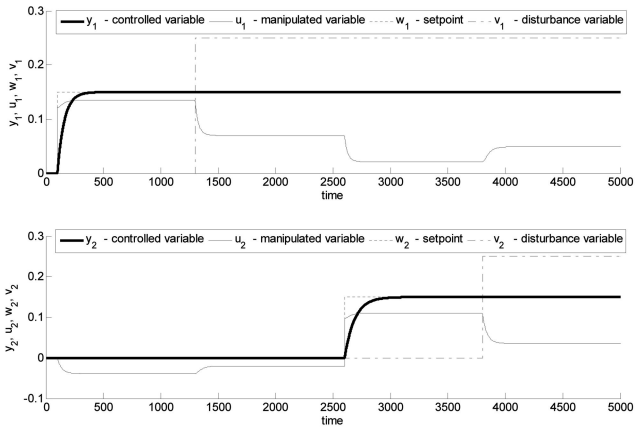

FIGURE 23. Control responses for operating point P_1 when using primary controller (81) tuned by the BTM, with auxiliary controllers *RP* (75) and correction members *KC* (87) providing absolute invariance of the control loop.

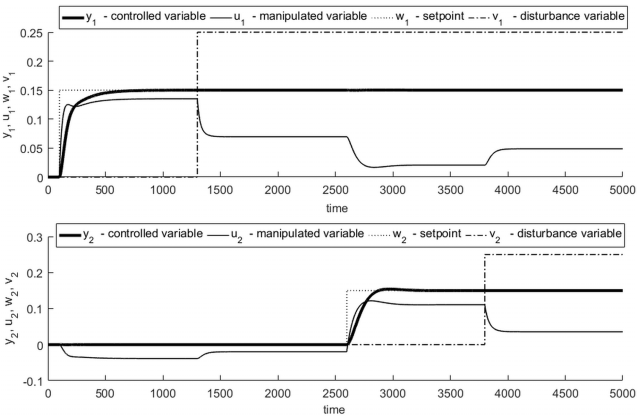

FIGURE 24. Control responses for operating point P_1 when using primary controller (82) tuned by the BTM, with filtered decoupler (77) ($T_F = 1$) and correction members *KC* (87) providing absolute invariance of the control loop.

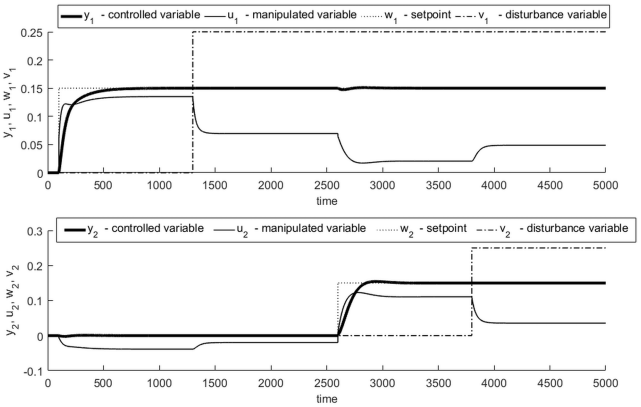

FIGURE 25. Control responses for operating point P_1 when using primary controller (83) tuned by the BTM, with filtered decoupler (78) ($T_F = 10$) and correction members *KC* (87) providing absolute invariance of the control loop.

b: OPERATING POINT P_2

In Figs. 30 – 39, control responses for the operating point P_2 when using the proposed method are displayed. None decouplers, primary controllers (94), (95), and none or only approximate correction members are assumed in Figs 30-33. In Figs 34-36, filtered decoupler (90) and primary

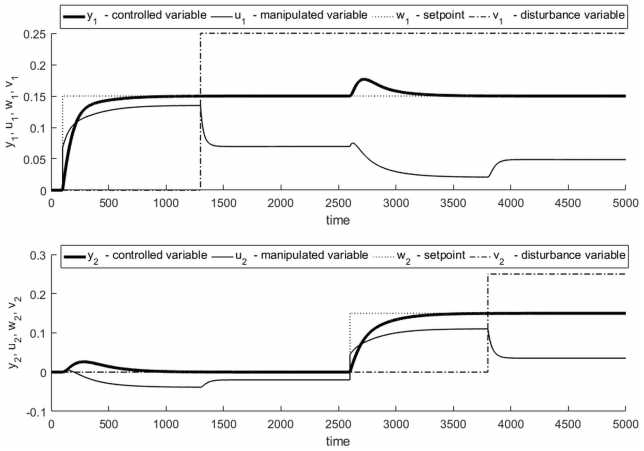

FIGURE 26. Control responses for operating point P_1 when using primary controller (84) tuned by the BTM, with simplified decoupler (79) and correction members *KC* (87) providing absolute invariance of the control loop.

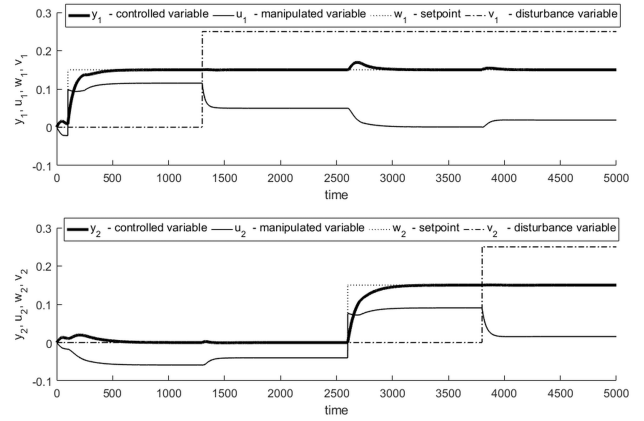

FIGURE 27. Control responses for operating point P_1 when using primary controller (81) tuned by the BTM, with fuzzy decoupler and correction members *KC* (87) providing absolute invariance of the control loop.

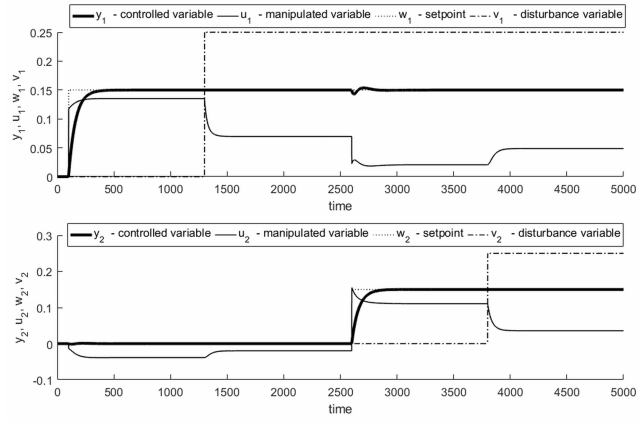

FIGURE 28. Control responses for operating point P_1 when using centralized inverted PI decoupling controller (85), with correction members *KC* (87) providing absolute invariance of the control loop.

controller (96) are combined with various $\boldsymbol{G}_{KC}(s)$. Similarly, another filtered decoupler (91) followed by controller (97) is applied for Figs. 37-39.

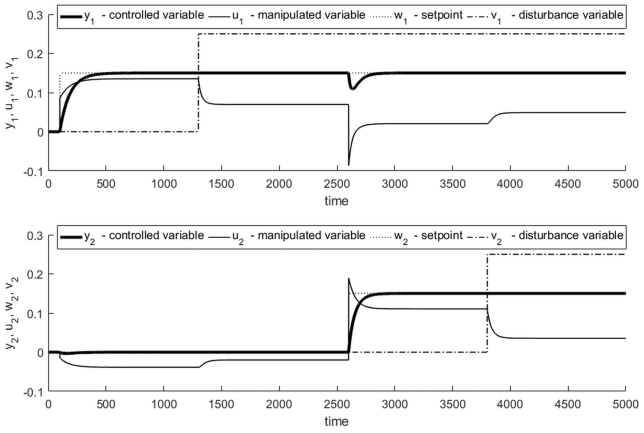

FIGURE 29. Control responses for operating point P_1 when using centralized controller (86) obtained via the polynomial design approach, with correction members *KC* (87) providing absolute invariance of the control loop.

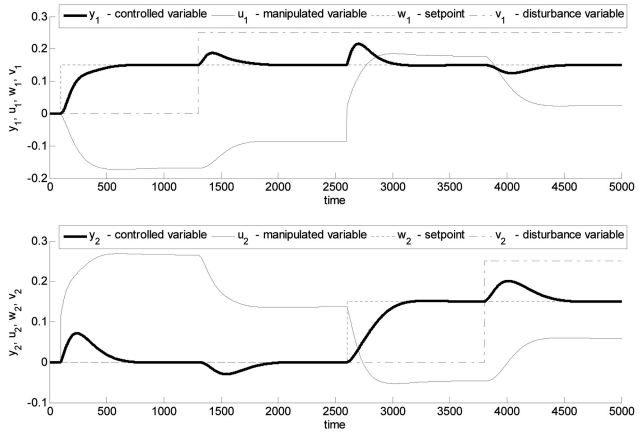

FIGURE 30. Control responses for operating point P_2 when using only primary controller (94) tuned by the MOM, i.e., without auxiliary controllers *RP* and correction members *KC*.

However, the use of the standard inverted decoupler (92) within the 2-1 configuration (or equivalently, the proposed modified inverted decoupler according to the Proposition 1) and primary controller (95) gives stable output responses, whereas the control action is unstable. This issue is discussed in Subsection III.D.

Control responses for simplified decoupler (93) with the primary controller (98) are given in Figs. 40 and 41. The fuzzy decoupler combined with the primary controller (95) yields responses as in Figs. 42 and 43. Simulation results for the centralized inverted PI decoupling controller (99) are provided in Figs. 44 and 45. Finally, the use of the centralized polynomial approach with the primary controller transfer function matrix (100) gives responses shown in Figs. 46 and 47.

Note that for all the above-introduced comparative results, the compensated and approximate correction members (102) and (103), respectively, are used.

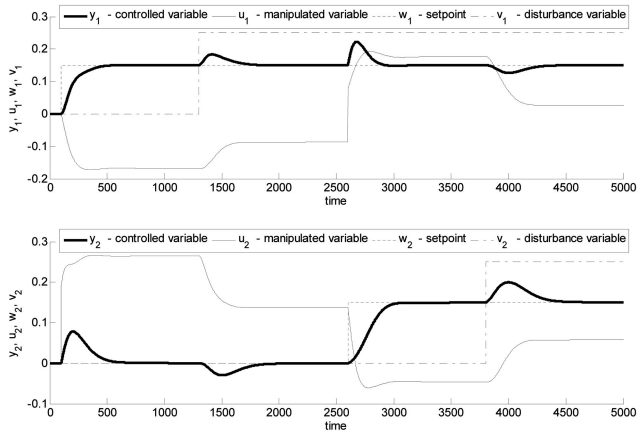

FIGURE 31. Control responses for operating point P_2 when using only primary controller (95) tuned by the DMM, i.e., without auxiliary controllers *RP* and correction members *KC*.

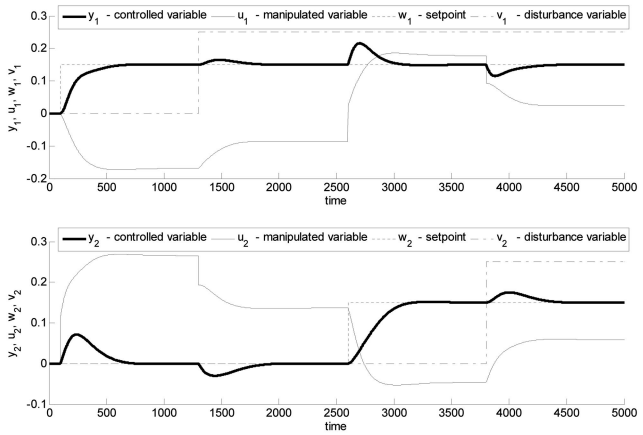

FIGURE 32. Control responses for operating point P_2 when using primary controller (94) tuned by the MOM, without auxiliary controllers *RP* yet with correction members *KC* (103) providing approximate invariance of the control loop.

D. SIMULATIONS EVALUATION AND DISCUSSION

The Integral Square Error (ISE) (104) and the Integral Time Absolute Error ITAE (105) criteria are used to evaluate simulation results provided to the reader in Figs. 18 to 47.

$$J_{\mathrm{ISE}} = \int_0^{\infty} e^2(t)\,dt \approx \int_0^{t_S} e^2(t)\,dt \tag{104}$$

$$J_{\mathrm{ITAE}} = \int_0^{\infty} t \cdot |e(t)|\,dt \approx \int_0^{t_S} t \cdot |e(t)|\,dt \tag{105}$$

In (104) and (105), $e(t) = w(t) - y(t)$ is the control error and t_s expresses the total simulation time (see Fig. 48). In addition, the control performance is measured by means of the control (settling) time t_r and via error peak values $e_{\max,w}$ and $e_{\max,d}$ as well which mean the maximum absolute value of $e(t)$ (i.e., the peak overshoot) due to setpoint change and disturbance entrance (even cross-interconnected ones), respectively. The value of δ is set to 2%.

TABLE 3. Performance of simulated control responses for two-variable control loop and operating point P_1.

Fig. No.	$J_{\mathrm{ISE},1}$	$J_{\mathrm{ITAE},1}$	$t_{r,1}$	$e_{\max,w,1}$	$e_{\max,d,1}$
Fig. 18	2.439	$5.645\cdot10^4$	597	0.024	0.045
Fig. 19	0.812	$2.688\cdot10^4$	318	0.021	0.025
Fig. 20	2.161	$4.325\cdot10^4$	597	0.022	0.020
Fig. 21	0.739	$2.056\cdot10^4$	318	0.019	0.008
Fig. 22	1.980	$4.043\cdot10^3$	494	0.007	0
Fig. 23	0.667	$1.401\cdot10^3$	229	0	0
Fig. 24	1.065	$3.303\cdot10^3$	475	0.001	0
Fig. 25	0.900	$4.151\cdot10^3$	457	0.001	0
Fig. 26	0.591	$1.193\cdot10^3$	206	0.027	0
Fig. 27	0.617	$1.469\cdot10^4$	366	0.019	0.005
Fig. 28	0.667	$3.370\cdot10^3$	236	0.002	0
Fig. 29	1.062	$1.141\cdot10^4$	339	0.042	0
Fig. No.	$J_{\mathrm{ISE},2}$	$J_{\mathrm{ITAE},2}$	$t_{r,2}$	$e_{\max,w,2}$	$e_{\max,d,2}$
Fig. 18	3.846	$1.603\cdot10^5$	476	0.031	0.052
Fig. 19	1.258	$7.880\cdot10^4$	439	0.017	0.031
Fig. 20	3.213	$9.894\cdot10^4$	476	0.032	0.011
Fig. 21	1.093	$4.844\cdot10^4$	438	0.018	0.004
Fig. 22	2.960	$8.244\cdot10^4$	737	0.007	0
Fig. 23	0.993	$3.542\cdot10^4$	343	0	0
Fig. 24	1.701	$4.756\cdot10^4$	451	0.004	0
Fig. 25	1.429	$4.182\cdot10^4$	428	0.004	0
Fig. 26	0.912	$3.290\cdot10^4$	322	0.017	0
Fig. 27	1.045	$4.241\cdot10^4$	462	0.020	0.003
Fig. 28	0.659	$2.382\cdot10^4$	238	0.007	0
Fig. 29	0.542	$2.134\cdot10^4$	221	0.004	0

It cannot be simply deduced what parameters give the optimal controller adjustment since there are contradictory requirements (integral criteria, shortest time criterion, overshoots) in the tables. Hence, a compromise between these multiple requirements ought to be found in practice.

The corresponding computed criteria values and other performance measures for P_1 and P_2 are displayed in Table 3 and Table 4, respectively. Note that the subscript number means the number of the output variable.

a: OPERATING POINT P_1

We do let evaluate the proposed method based on Table 3 (for operating point P_1) and compare it to the results of other methods.

Regarding the proposed method (or, the standard inverted decoupler), the beneficial effect of the use of auxiliary controllers (decouplers) and correction members can be deduced from Figs. 18-23. Overshoots caused by disturbances are reduced when using correction members. On the contrary, when only primary controllers are included in the control loop (Figs. 18 and 19), rather high overshoots are detected. The use of the BTM seems to be better options than the tuning based on the MOM.

Figs. 24 and 25 demonstrate the effect of non-optimal pairings to control response performance. All the performance criteria in Table 3 get worse. Moreover, as filtered decouplers have to be used here, control loops are partially coupled. The selected change of T_F does not influence responses significantly.

TABLE 4. Performance of simulated control responses for two-variable control loop and operating point P_2.

Fig. No.	$J_{\mathrm{ISE},1}$	$J_{\mathrm{ITAE},1}$	$t_{r,1}$	$e_{\max,w,1}$	$e_{\max,d,1}$
Fig. 30	2.789	$9.528\cdot10^4$	491	0.072	0.030
Fig. 31	2.274	$7.313\cdot10^4$	362	0.074	0.029
Fig. 32	2.625	$8.565\cdot10^4$	491	0.063	0.031
Fig. 33	2.159	$6.590\cdot10^4$	362	0.075	0.029
Fig. 34	5.254	$8.274\cdot10^4$	515	0.128	0.054
Fig. 35	5.447	$9.641\cdot10^4$	515	0.128	0.072
Fig. 36	5.704	$1.323\cdot10^5$	515	0.128	0.072
Fig. 37	11.154	$2.352\cdot10^5$	827	0.174	0.067
Fig. 38	10.889	$2.392\cdot10^5$	827	0.174	0.070
Fig. 39	13.105	$3.035\cdot10^5$	827	0.174	0.107
Fig. 40	6.294	$4.638\cdot10^4$	862	0.031	0.068
Fig. 41	17.335	$3.710\cdot10^5$	862	0.029	0.197
Fig. 42	3.765	$1.266\cdot10^5$	759	0.094	0.043
Fig. 43	4.881	$1.940\cdot10^5$	759	0.094	0.063
Fig. 44	7.732	$7.794\cdot10^4$	955	0.022	0.064
Fig. 45	10.866	$2.306\cdot10^5$	955	0.022	0.124
Fig. 46	5.682	$1.081\cdot10^5$	396	0.211	0.064
Fig. 47	6.546	$1.455\cdot10^5$	396	0.211	0.093
Fig. No.	$J_{\mathrm{ISE},2}$	$J_{\mathrm{ITAE},2}$	$t_{r,2}$	$e_{\max,w,2}$	$e_{\max,d,2}$
Fig. 30	5.147	$1.895\cdot10^5$	509	0.078	0.057
Fig. 31	4.648	$1.628\cdot10^5$	415	0.087	0.051
Fig. 32	4.627	$1.463\cdot10^5$	509	0.078	0.036
Fig. 33	4.216	$1.249\cdot10^5$	415	0.084	0.036
Fig. 34	4.965	$1.277\cdot10^5$	613	0.096	0.054
Fig. 35	5.200	$1.208\cdot10^5$	613	0.096	0.060
Fig. 36	5.198	$1.208\cdot10^5$	613	0.096	0.021
Fig. 37	2.218	$1.036\cdot10^5$	529	0.031	0.039
Fig. 38	2.249	$1.145\cdot10^5$	529	0.031	0.058
Fig. 39	2.321	$8.529\cdot10^4$	529	0.031	0.045
Fig. 40	7.147	$2.426\cdot10^5$	886	0.017	0.060
Fig. 41	16.967	$4.555\cdot10^5$	886	0.018	0.149
Fig. 42	3.278	$1.338\cdot10^5$	692	0.065	0.043
Fig. 43	3.660	$1.407\cdot10^5$	692	0.065	0.044
Fig. 44	7.170	$2.682\cdot10^5$	1075	0.019	0.056
Fig. 45	8.494	$2.335\cdot10^5$	1077	0.019	0.084
Fig. 46	1.505	$1.208\cdot10^5$	170	0.035	0.033
Fig. 47	1.683	$6.057\cdot10^4$	170	0.035	0.043

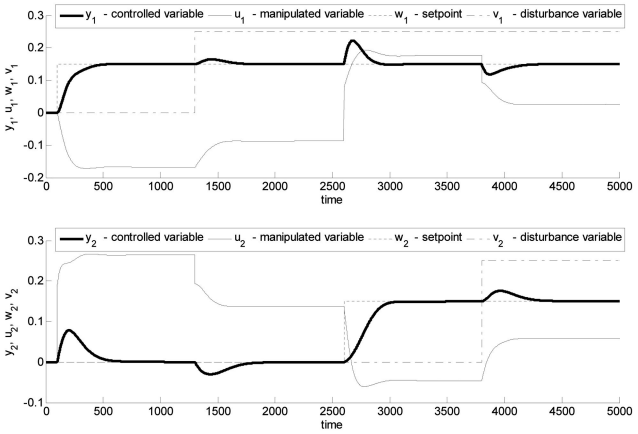

FIGURE 33. Control responses for operating point P_2 when using primary controller (95) tuned by the DMM, without auxiliary controllers *RP* yet with correction members *KC* (103) providing approximate invariance of the control loop.

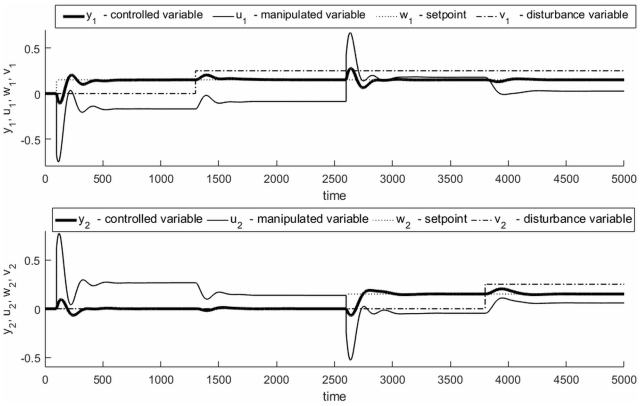

FIGURE 34. Control responses for operating point P_2 when using primary controller (96) tuned by the DMM, with filtered decoupler (90) yet without correction members *KC*.

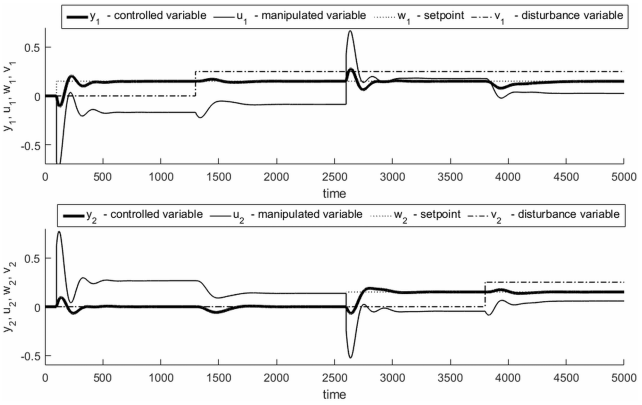

FIGURE 35. Control responses for operating point P_2 when using primary controller (96) tuned by the DMM, with filtered decoupler (90) and compensated correction members *KC* (102).

The use of the simplified decoupler (see Fig. 26) provides almost the worst decoupling for P_1; nevertheless, the invariance remains excellent.

The design of the fuzzy decoupler requires a priori knowledge of the range of the manipulated input values and the fuzzy rules setting is the matter of experience and erudition. Moreover, only mean criteria values are obtained (see Fig. 27) with a low level of loop interaction reduction.

Very good results are obtained by using the centralized inverted PI decoupling controller (see Fig. 28), offering a little less performance for y_1 (yet a slightly better one for y_2) compared to the proposed method. However, a partial coupling appears here.

Finally, the centralized polynomial approach gives an excellent result for y_2; however, those for y_1 are below-average. In addition, strong interactions between loops remain.

b: OPERATING POINT P_2

The assessment of the considered approaches for P_2 (giving rise to a non-minimum phase system) based on data in Table 4 is not so straightforward. The effect of various disturbance invariance strategies has to be evaluated as well.

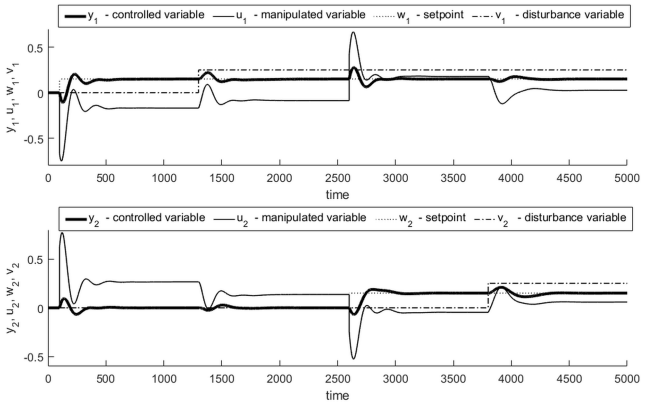

FIGURE 36. Control responses for operating point P_2 when using primary controller (96) tuned by the DMM, with filtered decoupler (90) and correction members *KC* (103) providing approximate invariance of the control loop.

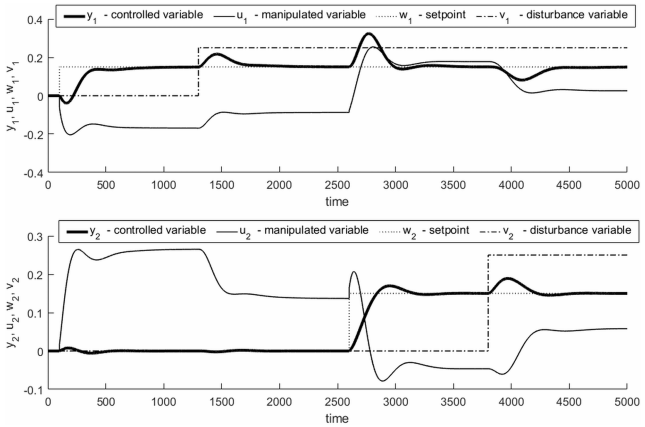

FIGURE 37. Control responses for operating point P_2 when using primary controller (97) tuned by the DMM, with filtered decoupler (91) yet without correction members *KC*.

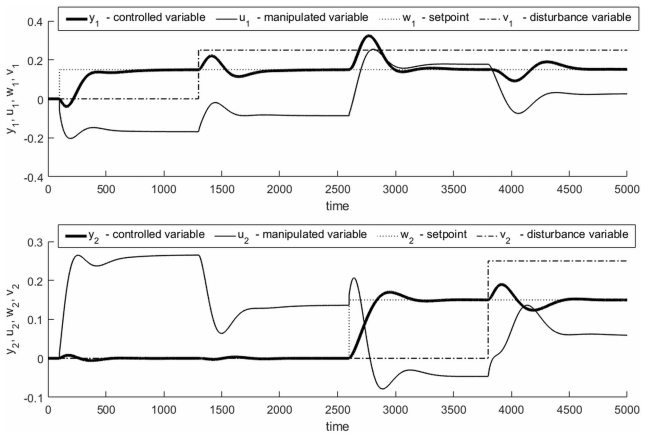

FIGURE 38. Control responses when operating point P_2 when using primary controller (97) tuned by the DMM, with filtered decoupler (91) and compensated correction members *KC* (102).

As mentioned in the preceding section, the use of the proposed ideal decoupler (or, the standard inverted decoupler) results in the unstable control action. This issue

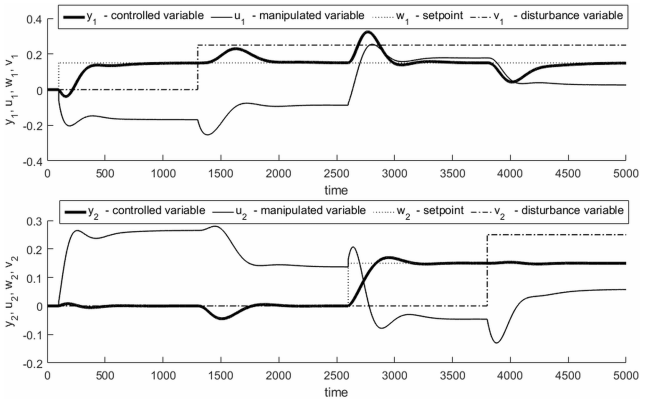

FIGURE 39. Control responses for operating point P_2 when using primary controller (97) tuned by the DMM, with filtered decoupler (91) and correction members *KC* (103) providing approximate invariance of the control loop.

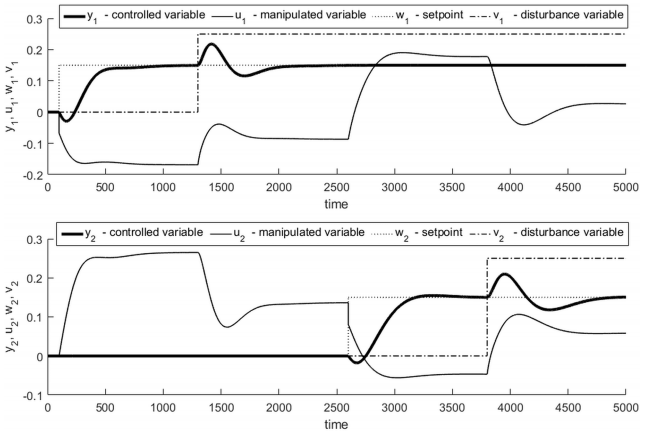

FIGURE 40. Control responses for operating point P_2 when using primary controller (98) tuned by the DMM, with simplified decoupler (93) and compensated correction members *KC* (102).

can be explained in the light of transfer function matrix $\boldsymbol{G}_{W/U}(s)$ of the reference signal to the manipulated input

$$\boldsymbol{G}_{W/U}(s) = \boldsymbol{G}_S(s)^{-1}\left[\boldsymbol{I}+\boldsymbol{G}_S(s)(\boldsymbol{I}+\boldsymbol{G}_{RP}(s))^{-1}\boldsymbol{G}_R(s)\right]^{-1} \cdot \boldsymbol{G}_S(s)\,(\boldsymbol{I}+\boldsymbol{G}_{RP}(s))^{-1}\boldsymbol{G}_R(s) \quad (106)$$

Hence, as the controlled system is non-minimum phase (i.e., polynomial $\det(\boldsymbol{G}_S(s))$ has some its roots in the RHP), the inverse of $\boldsymbol{G}_S(s)$ yields instability of (106).

In Figs. 30-33, the decoupler is not used and correction members are absent or they only ensure an approximate invariance. Surprisingly, the use of such correction members does not enhance disturbance responses. It can also be stated that primary controllers tuned via the DDM yields better performance than the use of the MOM.

Non-feasibility of the ideal decoupler and instability of the correction members for absolute invariance can be solved in the sense of compensator (35). The effect of such a solution is obvious from Figs. 34-39. Almost all the criteria displayed in Table 4 get worse, except for the y_2 response when using the filter with opposite gain signs (see Fig. 37-39). The control action is very high for decoupler (90). Moreover, the use

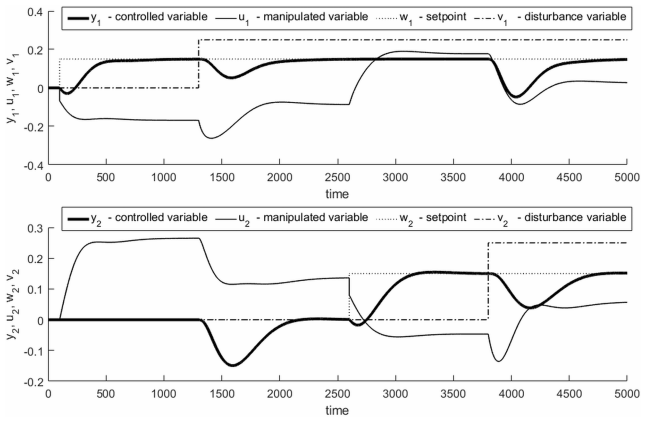

FIGURE 41. Control responses for operating point P_2 when using primary controller (98) tuned by the DMM, with simplified decoupler (93) and correction members *KC* (103) providing approximate invariance of the control loop.

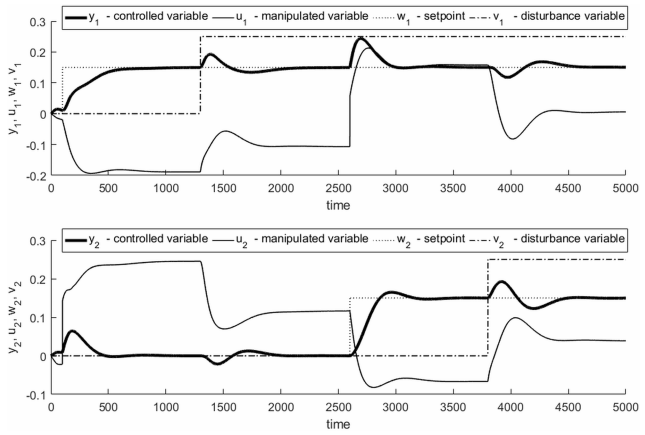

FIGURE 42. Control responses for operating point P_2 when using primary controller (95) tuned by the DMM, with fuzzy decoupler and compensated correction members *KC* (102).

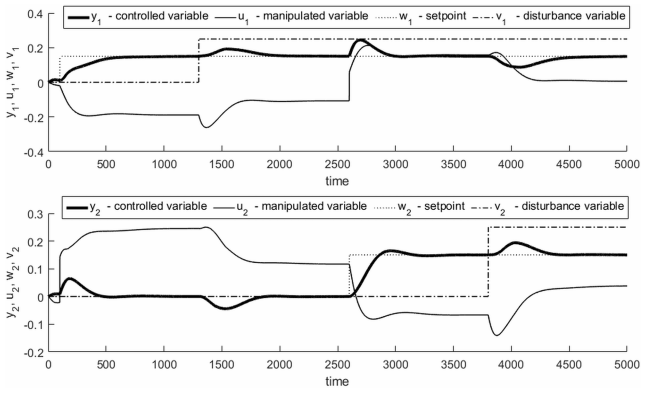

FIGURE 43. Control responses for operating point P_2 when using primary controller (95) tuned by the DMM, with fuzzy decoupler and correction members *KC* (103) providing approximate invariance of the control loop.

of correction members compared to their cancellation does not result in better disturbance responses, surprisingly.

The use of the simplified decoupler and correction members with unstable pole compensation gives a satisfactory disturbance attenuation only for non-crossed interactions

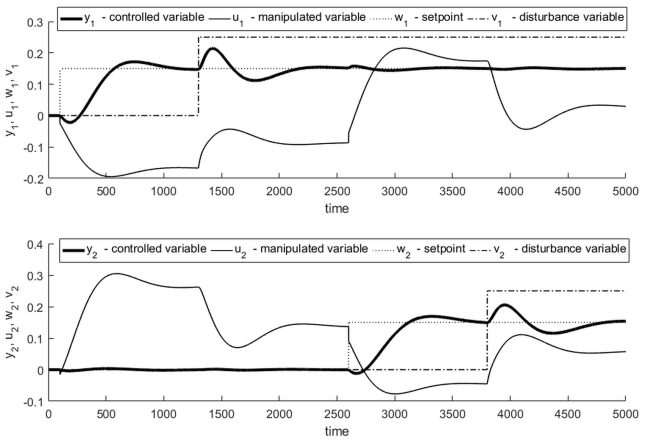

FIGURE 44. Control responses for operating point P_2 when using centralized inverted PI decoupling controller (99) and compensated correction members *KC* (102).

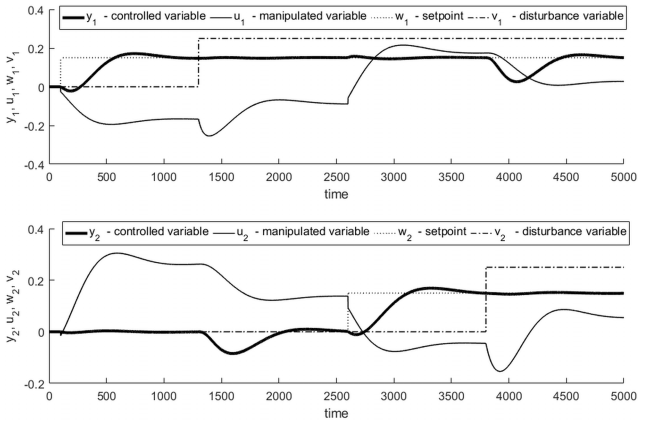

FIGURE 45. Control responses for operating point P_2 when using centralized inverted PI decoupling controller (99) and correction members *KC* (103) providing approximate invariance of the control loop.

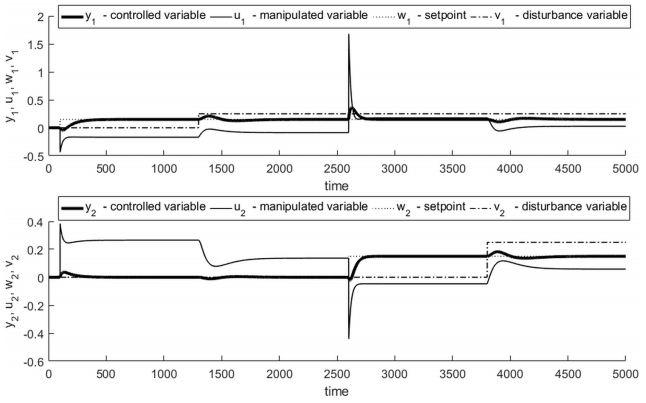

FIGURE 46. Control responses for operating point P_2 when using centralized controller (100) obtained via the polynomial design approach and compensated correction members *KC* (102).

(see Figs. 40 and 41). The crossed interactions yield poor invariance. Moreover, the settling time is long. Contrariwise, the level of decoupling is excellent.

Despite an obscure initial response, the use of the fuzzy decoupler results in very good integral performance measure values (Figs. 42 and 43).

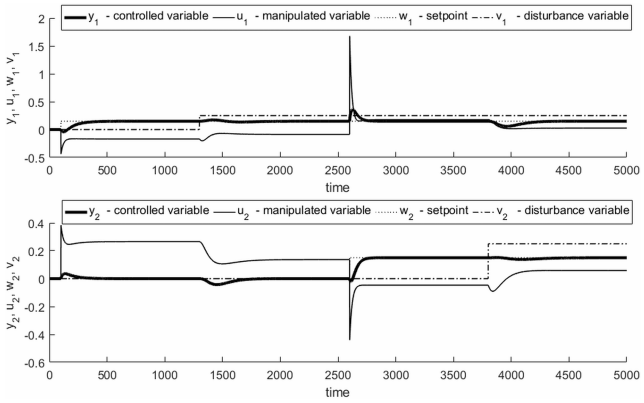

FIGURE 47. Control responses for operating point P_2 when using centralized controller (100) obtained via the polynomial design approach and correction members KC (103) providing approximate invariance of the control loop.

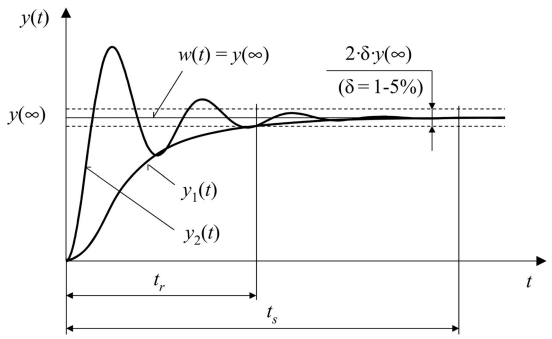

FIGURE 48. Control (output) response with the control time (t_r) and the simulation time (t_S).

The centralized inverted PI decoupling controller (see Figs. 44 and 45) gives a very slow control response, which implies only mediocre ITAE criteria values; however, the loop interactions are attenuated very well. On the other hand, the reaction to disturbances is poor.

Control responses due to the polynomial approach suffer from inherently very poor decoupling and very high control action, see Figs. 46 and 47, which may lead to the wind-up effect and unreal fast actuator action, in practice. This effect can be overcome by different feedback-poles selection. However, the control action is then fast with good integral criteria values (see Table 4).

Thus, the general recommendation for the proposed technique is to abandon the use of compensator (35) when decoupler entries or correction members are unstable or non-feasible. On the contrary, other benchmarked methods indicate the beneficial effect of compensated correction members.

To sum up, based on the general description of the proposed method and numerical results given above, the following advantages of the method can be formulated.

1) It provides the original combination of control structure selection techniques, inverted decoupler, disturbance rejection or attenuation, and primary control design.
2) It is simple and provides explicit formulae to design auxiliary controllers and correction members.
3) Despite the TITO simulation example, it has been verified up to the 5×5 dimension.
4) Simulation experiments have verified a very good performance compared to some other MIMO control techniques and non-optimal pairings.

Contrariwise, the disadvantages can be summarized as follows.

1) The direct application of the method to non-minimum phase or delayed systems brings about the necessity of the use of the compensation of unstable poles or non-feasible transfer function elements.
2) As indicated above, the use of modified decoupler and simplified or compensated correction members may yield worse control performance in some cases.
3) The method is applicable to only square MIMO systems (with a possibly non-square disturbance-to-output transfer function matrix) and it has been proved to the dimension 5×5 or less.
4) It cannot be used to nonlinear or discrete-time multivariable systems (e.g., multi-agent systems [107], [108]).

IV. CONCLUSION

This work has been aimed at the description of a control design method for MIMO control loops. It utilizes several tools and their combinations to determine dominant (i.e., optimally paired) elements of the controlled plant transfer matrix $\boldsymbol{G}_S(s)$; namely, the RGA, the RNGA, the NI tool, and the CN tool. These techniques are used to get the optimal control configuration selection for measurable disturbance variables transfer function $\boldsymbol{G}_{SV}(s)$ as well.

Once the optimal pairs are determined, entries of the proposed inverted decoupler, represented by the auxiliary controller transfer matrix $\boldsymbol{G}_{RP}(s)$, are appropriately set. Besides transition from the open-loop to closed-loop control system and advantage of a generally inverted decoupler, the introduction of the proposed decoupling scheme has also been motivated by an analogy to correction members for an approximate invariance (see Fig. 4 and equation (52)). In fact, the correction members take care of the cancellation of the effect of dominant disturbance pairs. Then, the effect of non-optimal pairs in the control loop can be reduced by using $\boldsymbol{G}_{RP}(s)$ analogously, as they were disturbance-output pairs.

Any SISO synthesis method can be then applied to design the parameters of entries of $\boldsymbol{G}_R(s)$ for the corresponding dominant elements $\boldsymbol{G}_S(s)$. Moreover, absolute or approximate invariance to disturbances in a MIMO control loop can be satisfied by the setting of individual entries (correction members) of $\boldsymbol{G}_{KC}(s)$. Whenever some of the calculated controllers are unstable or non-feasible (e.g., due to time delays), a compensation technique is suggested to overcome these issues.

The advantage of the proposed method is that a change of parameters in individual elements of the primary controller

transfer function matrix $\boldsymbol{G}_R(s)$ (e.g., due to the use of another SISO tuning method) does not influence entries of the auxiliary controller transfer function matrix $\boldsymbol{G}_{RP}(s)$ and correction members $\boldsymbol{G}_{KC}(s)$.

The reader has also been provided with a detailed numerical example of control of the two-variable quadruple-tank process to verify theoretical assumptions. A rich comparative study with selected MIMO system control methods has been made as well. The results are evaluated via several criteria. The advantages and disadvantages of the proposed method have been formulated based on its general properties and also on these numerical results. It can be stated that the method gives better (or at least comparable) results than the benchmarked ones.

The extension of the proposed method to non-square or arbitrary-dimension MIMO systems constitutes a challenging task for future research.

REFERENCES

[1] J. Balátě, *Automatic Control*, 2nd ed. Prague, Czech Republic: BEN, 2004.

[2] L. Jingyun and L. Ping, "Temperature and humidity control with a model predictive control method in the air-conditioning system," in *Proc. Int. Conf. Adv. Mech. Syst. (ICAMechS)*, Xiamen, China, Dec. 2017, pp. 408–412, doi: 10.1109/ICAMechS.2017.8316508.

[3] J. Vojtěšek and L. Spaček, "Adaptive control of temperature inside plug-flow chemical reactor using 2DOF controller," in *Innovation, Engineering and Entrepreneurship* (Lecture Notes in Computer Science). Guimaraes, Portugal: Springer-Verlag, 2019, pp. 103–109, doi: 10.1007/978-3-319-91334-6_15.

[4] D. Del Vecchio and N. Petit, "Boundary control for an industrial underactuated tubular chemical reactor," *J. Process Control*, vol. 15, no. 7, pp. 771–784, Oct. 2005, doi: 10.1016/j.jprocont.2005.03.004.

[5] K. Peng, D. Fan, F. Yang, L. Gou, and W. Lv, "A frequency domain decoupling method and multivariable controller design for turbofan engines," *IEEE Access*, vol. 5, pp. 27757–27766, 2017, doi: 10.1109/ACCESS.2017.2766838.

[6] L. Pekař and R. Prokop, "Algebraic robust control of a closed circuit heating-cooling system with a heat exchanger and internal loop delays," *Appl. Therm. Eng.*, vol. 113, pp. 1464–1474, Feb. 2017, doi: 10.1016/j.applthermaleng.2016.11.150.

[7] A. Kot and A. Nawrocka, "Balanced platform vibration control," *J. Low Freq. Noise, Vib. Active Control*, vol. 32, no. 3, pp. 227–238, Sep. 2013, doi: 10.1260/0263-0923.32.3.227.

[8] C. Kasnakoğlu, "Investigation of multi-input multi-output robust control methods to handle parametric uncertainties in autopilot design," *PLoS ONE*, vol. 11, no. 10, Oct. 2016, Art. no. e0165017, doi: 10.1371/journal.pone.0165017.

[9] F. Šolc, "Modelling and control of a quadrocopter," *AiMT*, vol. 5, no. 2, pp. 29–38, Dec. 2010.

[10] B. Tian, L. Liu, H. Lu, Z. Zuo, Q. Zong, and Y. Zhang, "Multivariable finite time attitude control for quadrotor UAV: Theory and experimentation," *IEEE Trans. Ind. Electron.*, vol. 65, no. 3, pp. 2567–2577, Mar. 2018, doi: 10.1109/TIE.2017.2739700.

[11] S. Gong, B. Yin, Z. Zheng, and K. Cai, "Adaptive multivariable control for multiple resource allocation of service-based systems in cloud computing," *IEEE Access*, vol. 7, pp. 13817–13831, Jan. 2019, doi: 10.1109/ACCESS.2019.2894188.

[12] K. Warwick and D. Rees, *Industrial Digital Control Systems* (IEE Control Engineering Series), vol. 37. London, U.K.: Peter Peregrinus, 1988.

[13] K. H. Johansson, "The quadruple-tank process: A multivariable laboratory process with an adjustable zero," *IEEE Trans. Control Syst. Technol.*, vol. 8, no. 3, pp. 456–465, May 2000, doi: 10.1109/87.845876.

[14] D. D. Šiljak, "Decentralized control and computations: Status and prospects," *Annu. Rev. Control*, vol. 20, pp. 131–141, Jan. 1996, doi: 10.1016/S1367-5788(97)00011-4.

[15] A. İftar and E. J. Davison, "Decentralized control strategies for dynamic routing," *Optim. Control Appl. Methods*, vol. 23, no. 6, pp. 329–355, Nov. 2002, doi: 10.1002/oca.717.

[16] L. Bakule, "Decentralized control: An overview," *IFAC Proc.*, vol. 40, no. 9, pp. 39–48, Jul. 2007, doi: 10.3182/20070723-3-PL-2917.00006.

[17] A. Y. Sendjaja and V. Kariwala, "Minimum variance benchmark for performance assessment of decentralized controllers," *Ind. Eng. Chem. Res.*, vol. 51, no. 11, pp. 4288–4298, 2012, doi: 10.1021/ie201361d.

[18] A. Khaki-Sedigh and B. Moaveni, *Control Configuration Selection for Multivariable Plants*. (Lecture Notes in Control and Information Sciences), vol. 391. Berlin, Germany: Springer-Verlag, 2009.

[19] M. Kinnaert, "Interaction measures and pairing of controlled and manipulated variables for multiple-input multiple-output systems: A survey," *J. A*, vol. 36, no. 4, pp. 15–23, 1995.

[20] B. Halvarsson, "Interaction analysis in multivariable control systems: Applications to bioreactors for nitrogen removal," Ph.D. dissertation, Fac. Sci. Technol., Uppsala Univ., Uppsala, Sweden, 2010.

[21] M. S. Chiu and Y. Arkun, "Decentralized control structure selection based on integrity considerations," *Ind. Eng. Chem. Res.*, vol. 29, no. 3, pp. 369–373, Mar. 1990, doi: 10.1021/ie00099a012.

[22] M.-J. He, W.-J. Cai, W. Ni, and L.-H. Xie, "RNGA based control system configuration for multivariable processes," *J. Process Control*, vol. 19, no. 6, pp. 1036–1042, Jun. 2009, doi: 10.1016/j.jprocont.2009.01.004.

[23] X. Luan, Q. Chen, and F. Liu, "Interaction measurement for complex multivariable models with various reference inputs based on RNGA," in *Proc. 11th Asian Control Conf. (ASCC)*, Gold Coast, QLD, Australia, Dec. 2017, pp. 2411–2416, doi: 10.1109/ASCC.2017.8287552.

[24] M. Van de Wal and B. de Jager, "A review of methods for input/output selection," *Automatica*, vol. 37, no. 4, pp. 487–510, Apr. 2001.

[25] A. Jain and B. V. Babu, "Sensitivity of relative gain array for processes with uncertain gains and residence times," *IFAC-PapersOnLine*, vol. 49, no. 1, pp. 486–491, Apr. 2016, doi: 10.1016/j.ifacol.2016.03.101.

[26] E. Bristol, "On a new measure of interaction for multivariable process control," *IEEE Trans. Autom. Control*, vol. AC-11, no. 1, pp. 133–134, Jan. 1966, doi: 10.1109/TAC.1966.1098266.

[27] V. Manousiouthakis, R. Savage, and Y. Arkun, "Synthesis of decentralized process control structures using the concept of block relative gain," *AIChE J.*, vol. 32, no. 6, pp. 991–1003, Jun. 1986, doi: 10.1002/aic.690320609.

[28] K. E. Häggblom, "Partial relative gain: A new tool for control structure selection," in *Proc. Eur. Control Conf. (ECC)*, Brussels, Belgium, Jul. 1997, doi: 10.23919/ECC.1997.7082571.

[29] M. Witcher and T. J. McAvoy, "Interacting control systems: Steady state and dynamic measurement of interactions," *ISA Trans.*, vol. 16, no. 3, pp. 35–41, 1977.

[30] T. J. McAvoy, "Some results on dynamic interaction analysis of complex control systems," *Ind. Eng. Chem. Process Des. Devices*, vol. 22, no. 1, pp. 42–49, Jan. 1983, doi: 10.1021/i200020a008.

[31] T. J. McAvoy, Y. Arkun, R. Chen, D. Robinson, and P. D. Schnelle, "A new approach to defining a dynamic relative gain," *Control Eng. Pract.*, vol. 11, no. 8, pp. 907–914, Aug. 2003, doi: 10.1016/S0967-0661(02)00207-1.

[32] Q. Xiong, W.-J. Cai, and M.-J. He, "A practical loop pairing criterion for multivariable processes," *J. Process Control*, vol. 15, no. 7, pp. 741–747, Oct. 2005, doi: 10.1016/j.jprocont.2005.03.008.

[33] Z. X. Zhu, "Variable pairing selection based on individual and overall interaction measures," *Ind. Eng. Chem. Res.*, vol. 35, no. 11, pp. 4091–4099, Nov. 1996, doi: 10.1021/ie960143n.

[34] A. Fatehi and A. Shariati, "Automatic pairing of MIMO plants using normalized RGA," in *Proc. Medit. Conf. Control Autom.*, Athens, Greece, Jun. 2007, pp. 1–6, doi: 10.1109/MED.2007.4433929.

[35] A. Balestrino, E. Crisostomi, A. Landi, and A. Menicagli, "ARGA loop pairing criteria for multivariable systems," in *Proc. 47th IEEE Conf. Decis. Control (CDC)*, Cancun, Mexico, Dec. 2008, pp. 5568–5673, doi: 10.1109/CDC.2008.4738840.

[36] B. Halvarsson, B. Carlsson, and T. Wik, "A new input/output pairing strategy based on linear quadratic Gaussian control," in *Proc. IEEE Int. Conf. Control Autom. (ICCA)*, Christchurch, New Zealand, Dec. 2009, pp. 978–982, doi: 10.1109/ICCA.2009.5410387.

[37] A. Avvalabadi and A. Shahmansourian, "A new mathematical approach for input-output pairing in MIMO square systems," in *Proc. 22nd Iranian Conf. Electr. Eng. (ICEE)*, Tehran, Iran, May 2014, pp. 1244–1247, doi: 10.1109/IranianCEE.2014.6999725.

[38] V. Huilcapi, X. Blasco, J. M. Herrero, and G. Reynoso-Meza, "A loop pairing method for multivariable control systems under a multi-objective optimization approach," *IEEE Access*, vol. 7, pp. 81994–82014, Jun. 2019.
[39] A. M. H. Kadhim, "Selection of decentralized control configuration for uncertain systems," Ph.D. dissertation, Dept. Comput. Sci., Elect. Space Eng., Luleå Univ. Technol., Luleå, Sweden, 2018.
[40] Q. Liao and D. Sun, "Interaction measures for control configuration selection based on interval type-2 Takagi–Sugeno fuzzy model," *IEEE Trans. Fuzzy Syst.*, vol. 26, no. 5, pp. 2510–2523, Oct. 2018, doi: 10.1109/TFUZZ.2018.2791929.
[41] J. Zhang, Y. Kuai, M. Lin, R. Wang, and G. Hou, "Coupling analysis and loop pairing method via an information-theoretic approach," in *Proc. IEEE 11th Conf. Ind. Electron. Appl. (ICIEA)*, Hefei, China, Jun. 2016, pp. 1939–1944, doi: 10.1109/ICIEA.2016.7603905.
[42] C. H. Liu, *General Decoupling Theory of Multivariable Process Control Systems*. Berlin, Germany: Springer-Verlag, 1983.
[43] Q. G. Wang, *Decoupling Control*, vol. 285. Berlin, Germany: Springer-Verlag, 2003.
[44] J. L. Chang, "Discrete-time PID observer design for state and unknown input estimations in noisy measurements," *Int. J. Control Autom.*, vol. 13, no. 4, pp. 816–822, May 2015, doi: 10.1007/s12555-014-0151-z.
[45] L. Liu, S. Tian, D. Xue, T. Zhang, Y. Q. Chen, and S. Zhang, "A review of industrial MIMO decoupling control," *Int. J. Control Autom.*, vol. 17, no. 5, pp. 1246–1254, May 2019, doi: 10.1007/s12555-018-0367-4.
[46] J. Lee, D. H. Kim, and T. F. Edgar, "Static decouplers for control of multivariable processes," *AIChE J.*, vol. 51, no. 10, pp. 2712–2720, Jul. 2005, doi: 10.1002/aic.10520.
[47] E. Gagnon, A. Pomerleau, and A. Desbiens, "Simplified, ideal or inverted decoupling?" *ISA Trans.*, vol. 37, no. 4, pp. 265–276, Sep. 1998, doi: 10.1016/S0019-0578(98)00023-8.
[48] D. A. Vijula and N. Devarajan, "Decentralized PI controller design for non linear multivariable systems based on ideal decoupler," *J. Theor. Appl. Inf. Technol.*, vol. 64, no. 2, pp. 568–574, Jun. 2014.
[49] L. Yunhui, L. Hongbo, and J. Lei, "Improved inverted decoupling control using dead-time compensator for MIMO processes," in *Proc. IEEE 29th Chin. Control Conf.*, Beijing, China, Jul. 2010, pp. 3548–3553.
[50] W. L. Luyben, "Distillation decoupling," *AIChE J.*, vol. 16, no. 2, pp. 198–203, Mar. 1970, doi: 10.1002/aic.690160209.
[51] M. Waller, J. B. Waller, and K. V. Waller, "Decoupling revisited," *Ind. Eng. Chem. Res.*, vol. 42, no. 20, pp. 4575–4577, Jul. 2003, doi: 10.1021/ie020911c.
[52] S. Xu, S. Hashimioto, W. Jiang, Y. Jiang, K. Izaki, T. Kihara, and R. Idea, "Slow mode-based control method for multi-point temperature control system," *Processes*, vol. 7, Aug. 2019, Art. no. 553, doi: 10.3390/pr7080533.
[53] F. G. Shinskey, *Process Control Systems: Application, Design, and Tuning*. New York, NY, USA: McGraw-Hill, 1990.
[54] H. L. Wade, "Inverted decoupling: A neglected technique," *ISA Trans.*, vol. 36, no. 1, pp. 3–10, May 1997, doi: 10.1016/S0019-0578(97)00008-6.
[55] P. Chen and W. Zhang, "Improvement on an inverted decoupling technique for a class of stable linear multivariable processes," *ISA Trans.*, vol. 46, no. 2, pp. 199–210, Apr. 2007, doi: 10.1016/j.isatra.2006.09.002.
[56] J. Garrido, F. Vázquez, and F. Morilla, "An extended approach of inverted decoupling," *J. Process Control*, vol. 21, no. 1, pp. 55–68, Jan. 2011, doi: 10.1016/j.jprocont.2010.10.004.
[57] J. Garrido, M. Lara, M. Ruz, F. Vázquez, J. Alfaya, and F. Morilla, "Decentralized PID control with inverted decoupling and superheating reference generation for efficient operation: Application to the benchmark PI 2018," *IFAC-PapersOnLine*, vol. 51, no. 4, pp. 710–715, 2018, doi: 10.1016/j.ifacol.2018.06.187.
[58] M. Noeding, J. Martensen, N. Lemke, W. Tegethoff, and J. Koehler, "Selection of decoupling control methods suited for automated design for uncertain TITO processes," in *Proc. IEEE 14th Int. Conf. Control Automat. (ICCA)*, Anchorage, AK, USA, Jun. 2018, pp. 498–505, doi: 10.1109/ICCA.2018.8444216.
[59] A. P. V. A. Aguiar, G. Acioli, Jr., and P. R. Barros, "Frequency domain evaluation and redesign of inverted decoupler," *IFAC-PapersOnLine*, vol. 52, no. 1, pp. 172–177, Jul. 2019, doi: 10.1016/j.ifacol.2019.06.056.
[60] S. R. Mahapatro, B. Subudhi, and S. Ghosh, "Design and experimental realization of a robust decentralized PI controller for a coupled tank system," *ISA Trans.*, vol. 89, pp. 158–168, Jun. 2019, doi: 10.1016/j.isatra.2018.12.003.
[61] X. Du and Q. Jin, "Modified disturbance observer-based control for stable multivariate processes with multiple time delays," *J. Process Control*, vol. 72, pp. 52–63, Nov. 2018, doi: 10.1016/j.jprocont.2018.10.005.
[62] J. Garrido, F. Vázquez, and F. Morilla, "Centralized inverted decoupling control," *Ind. Eng. Chem. Res.*, vol. 52, no. 23, pp. 7854–7866, May 2013, doi: 10.1021/ie400367m.
[63] M. Li and P. Zhou, "Analytical design based hierarchical control for non-square MIMO wood-chip refining process," *ISA Trans.*, vol. 90, pp. 52–63, Jul. 2019, doi: 10.1016/j.isatra.2018.12.045.
[64] J. Garrido, F. Vázquez, and F. Morilla, "Multivariable PID control by decoupling," *Int. J. Syst. Sci.*, vol. 47, no. 5, pp. 1054–1072, 2016, doi: 10.1080/00207721.2014.911390.
[65] C. Huang, W. H. Gui, C. Yang, and Y. Xie, "Design of decoupling Smith control for multivariable system with time delays," *J. Central South Univ.*, vol. 18, no. 2, pp. 473–478, Nov. 2011, doi: 10.1007/s11771-011-0720-8.
[66] T. Liu, W. Zhang, and F. Gao, "Analytical decoupling control strategy using a unity feedback control structure for MIMO processes with time delays," *J. Process Control*, vol. 17, no. 2, pp. 173–186, Feb. 2007, doi: 10.1016/j.jprocont.2006.08.010.
[67] S. A. C. Giraldo, R. C. C. Flesch, J. E. Normey-Rico, and M. Z. P. Sejas, "A method for designing decoupled filtered smith predictor for square MIMO systems with multiple time delays," *IEEE Trans. Ind. Appl.*, vol. 54, no. 6, pp. 6439–6449, Nov./Dec. 2018, doi: 10.1109/TIA.2018.2849365.
[68] Z. Deng, Y. Wang, F. Gu, and C. Li, "Robust decoupling control of BTT vehicle based on PSO," *Int. J. Bio-Inspired Comput.*, vol. 2, no. 1, pp. 42–50, Dec. 2009, doi: 10.1504/IJBIC.2010.030043.
[69] V. L. Chuong, T. N. L. Vu, N. T. N. Truong, and J. H. Jung, "An analytical design of simplified decoupling Smith predictors for multivariable processes," *Appl. Sci.*, vol. 9, Jun. 2019, Art. no. 2487, doi: 10.3390/app9122487.
[70] Y. Weng and X. Gao, "Adaptive sliding mode decoupling control with data-driven sliding surface for unknown MIMO nonlinear discrete systems," *Circuits Syst. Signal Process.*, vol. 36, no. 3, pp. 969–997, Jun. 2017, doi: 10.1007/s00034-016-0353-0.
[71] N. Van Chi, "Adaptive feedback linearization control for twin rotor multiple-input multiple-output system," *Int. J. Control, Automat. Syst.*, vol. 15, no. 3, pp. 1267–1274, 2017, doi: 10.1007/s12555-015-0245-2.
[72] Z. Liu, J. Du, H. Bao, and Q. Xu, "Adaptive reduced dimension fuzzy decoupling control method with its application to a deployable antenna panel," *Int. J. Aerosp. Eng.*, vol. 2018, Sep. 2018, Art. no. 4716863, doi: 10.1155/2018/4716863.
[73] M. Hamdy, A. Ramadan, and B. Abozalam, "Comparative study of different decoupling schemes for TITO binary distillation column via PI controller," *IEEE/CAA J. Automatica Sinica*, vol. 5, no. 4, pp. 869–877, Jul. 2018, doi: 10.1109/JAS.2016.7510040.
[74] Y. Fu and T. Chai, "Neural-network-based nonlinear adaptive dynamical decoupling control," *IEEE Trans. Neural Netw.*, vol. 18, no. 3, pp. 921–925, May 2007, doi: 10.1109/TNN.2007.891588.
[75] G. Liu, Z. Wang, C. Mei, and Y. Ding, "A review of decoupling control based on multiple models," in *Proc. 24th Chin. Control Decis. Conf. (CCDC)*, Taiyuan, China, May 2012, pp. 1077–1081, doi: 10.1109/CCDC.2012.6244171.
[76] B. T. Jevtović and M. R. Mataušek, "PID controller design of TITO system based on ideal decoupler," *J. Process Control*, vol. 20, no. 7, pp. 869–876, Aug. 2010, doi: 10.1016/j.jprocont.2010.05.006.
[77] C. Rajapandiyan and M. Chidambaram, "Controller design for MIMO processes based on simple decoupled equivalent transfer functions and simplified decoupler," *Ind. Eng. Chem. Res.*, vol. 51, no. 38, pp. 12398–12410, Aug. 2012, doi: 10.1021/ie301448c.
[78] P. Hušek, "Decentralized PI controller design based on phase margin specifications," *IEEE Trans. Control Syst. Technol.*, vol. 22, no. 1, pp. 346–351, Jan. 2014, doi: 10.1109/TCST.2013.2248060.
[79] P. P. Biswas, R. Srivastava, S. Ray, and A. N. Samanta, "Sliding mode control of quadruple tank process," *Mechatronics*, vol. 19, no. 4, pp. 548–561, Jun. 2009.
[80] X. Zhou, C. Li, T. Huang, and M. Xiao, "Fast gradient-based distributed optimisation approach for model predictive control and application in four-tank benchmark," *IET Control Theory Appl.*, vol. 9, no. 10, pp. 1579–1586, Jun. 2015, doi: 10.1049/iet-cta.2014.0549.
[81] P. Roy and B. K. Roy, "Dual mode adaptive fractional order PI controller with feedforward controller based on variable parameter model for quadruple tank process," *ISA Trans.*, vol. 63, pp. 365–376, Jul. 2016, doi: 10.1016/j.isatra.2016.03.010.

[82] W. Belhaj and O. Boubaker, "On MIMO PID control of the quadruple-tank process via ILMIs approaches: Minimum and non-minimum case studies," *IFAC Proc.*, vol. 46, no. 32, pp. 481–486, Dec. 2013, doi: 10.3182/20131218-3-IN-2045.00083.

[83] B. C. Reddy, M. Chidambaram, and M. K. D. Al-Gobaisi, "Design of centralized controllers for a MSF desalination plant," *Desalination*, vol. 113, no. 1, pp. 27–38, Nov. 1997, doi: 10.1016/S0011-9164(97)00112-4.

[84] A. Maxim, C. M. Ionescu, C. Copot, R. De Keyser, and C. Lazar, "Multivariable model-based control strategies for level control in a quadruple tank process," in *Proc. IEEE 17th Int. Conf. Syst. Theory, Control Comput. (ICSTCC)*, Sinaia, Romania, Oct. 2013, pp. 343–348, doi: 10.1109/ICSTCC.2013.6688983.

[85] A. Numsomran, T. Trisuwannawat, and V. Tipsuwanporn, "Adaptive fractional order PIλDμ control for multi-configuration tank process (MCTP) toolbox," *Int. J. Intell. Eng. Syst.*, vol. 11, no. 5, pp. 21–34, Oct. 2018, doi: 10.22266/ijies2018.1031.03.

[86] A. Niederlinski, "A heuristic approach to the design of linear multivariable interacting control systems," *Automatica*, vol. 7, no. 6, pp. 691–701, 1971, doi: 10.1016/0005-1098(71)90007-0.

[87] J. C. Jeng, *Multiloop and Multivariable Control*. Taipei, Taiwan: Nat. Taipei Univ. Technol., 2010.

[88] M. Hovd and S. Skogestad, "Simple frequency dependent tools for control system analysis, structure selection and design," *Automatica*, vol. 28, no. 5, pp. 989–996, Sep. 1992, doi: 10.1016/0005-1098(92)90152-6.

[89] K. Åström and T. Hägglund, *PID Controllers: Theory, Design and Tuning*, 2nd ed. Raleigh NC, USA: Instrument Society of America, 1995.

[90] A. O'Dwyer, *Handbook of PI and PID Controller Tuning Rules*, 3rd ed. London, U.K.: Imperial College Press, 2009.

[91] K. H. Ang, G. Chong, and Y. Li, "PID control system analysis, design, and technology," *IEEE Trans. Control Syst. Technol.*, vol. 13, no. 4, pp. 559–576, Jul. 2005, doi: 10.1109/TCST.2005.847331.

[92] V. Kučera, "Diophantine equations in control—A survey," *Automatica*, vol. 29, no. 6, pp. 1361–1375, Nov. 1993, doi: 10.1016/0005-1098(93)90003-C.

[93] E. N. Rosenwasser and B. P. Lampe, *Multivariable Computer-Controlled Systems: A Transfer Function Approach*. London, U.K.: Springer-Verlag, 2006.

[94] P. Klán and R. Gorez, "Balanced tuning of PI controllers," *Eur. J. Control*, vol. 6, no. 6, pp. 541–550, Nov. 2000, doi: 10.1016/S0947-3580(00)71117-4.

[95] R. Gorez and P. Klán, "Nonmodel-based explicit design relations for PID controllers," *IFAC Proc.*, vol. 33, no. 4, pp. 133–140, Apr. 2000, doi: 10.1016/S1474-6670(17)38233-2.

[96] L. Pekař and F. Gazdoš, "A potential use of the balanced tuning method for the control of a class of time-delay systems," in *Proc. 22nd Int. Conf. Process Control (PC)*, Strbske Pleso, Slovakia, Jun. 2019, pp. 161–166, doi: 10.1109/PC.2019.8815055.

[97] M. Vitečková and A. Víteček, "Modulus optimum for digital controllers," *Acta Montanistica Slovaca*, vol. 8, no. 4, pp. 214–216, 2003.

[98] T. Glad and L. Ljung, *Control Theory: Multivariable and Nonlinear Methods*. New York, NY, USA: Taylor & Francis, 2000.

[99] T. J. McAvoy, *Interaction Analysis: Principles and Applications*. Research Triangle, NC, USA: Instrument Society of America, 1986.

[100] W. Hu, W. J. Cai, and G. Xiao, "Decentralized control system design for MIMO processes with integrators/differentiators," *Ind. Eng. Chem. Res.*, vol. 49, no. 24, pp. 12521–12528, Oct. 2010, doi: 10.1021/ie1005838.

[101] P. Grosdidier, M. Morari, and B. R. Holt, "Closed-loop properties from steady-state gain information," *Ind. Eng. Chem. Fundamen.*, vol. 24, no. 2, pp. 221–235, May 1985, doi: 10.1021/i100018a015.

[102] S. Skogestad and I. Postlethwaite, *Multivariable Feedback Control: Analysis and Design*, 2nd ed. Chichester, U.K.: Wiley, 2005.

[103] K. W. Gwak and G. Y. Masada, "Structural analysis and optimization of nonlinear control systems using singular value decomposition," *J. Dyn. Syst. Meas. Control*, vol. 127, no. 1, pp. 105–113, Mar. 2005, doi: 10.1115/1.1876495.

[104] L. Pekař and Q. Gao, "Spectrum analysis of LTI continuous-time systems with constant delays: A literature overview of some recent results," *IEEE Access*, vol. 6, pp. 35457–35491, Jul. 2018, doi: 10.1109/ACCESS.2018.2851453.

[105] H. H. Rosenbrock, "Design of multivariable control systems using the inverse Nyquist array," *Proc. IEEE*, vol. 116, no. 11, pp. 1929–1936, Nov. 1969, doi: 10.1049/piee.1969.0354.

[106] H. H. Rosenbrock, *State-Space and Multivariable Theory*. London, U.K.: Nelson, 1970.

[107] R. Sakthivel, A. Parivallal, B. Kaviarasan, H. Lee, and Y. Lim, "Finite-time consensus of Markov jumping multi-agent systems with time-varying actuator faults and input saturation," *ISA Trans.*, vol. 83, pp. 89–99, Dec. 2018, doi: 10.1016/j.isatra.2018.08.016.

[108] R. Sakthivel, B. Kaviarasan, C. K. Ahn, and H. R. Karimi, "Observer and stochastic faulty actuator-based reliable consensus protocol for multiagent system," *IEEE Trans. Syst., Man., Cybern., Syst.*, vol. 48, no. 12, pp. 2383–2393, Dec. 2018, doi: 10.1109/TSMC.2017.2758902.

PAVEL NAVRÁTIL was born in Uherské Hradiště, Czech Republic, in 1976. He received the M.S. degree in automation and control technology in industry from the Faculty of Technology, Brno University of Technology, Zlín, Czech Republic, in 2000, and the Ph.D. degree in technical cybernetics from the Faculty of Applied Informatics, Tomas Bata University in Zlín, Czech Republic, in 2004.

He is currently a Senior Lecturer with the Faculty of Applied Informatics, Tomas Bata University in Zlín. He is the author or coauthor of 26 international conference contributions and journal articles. His research interests include analysis, synthesis, and simulation of single- and multivariable systems, monitoring and control of technological processes using programmable logic controllers and SCADA systems, and control algorithms in heat-production and heat-distribution networks.

LIBOR PEKAŘ was born in Zlín, Czech Republic, in 1979. He received the B.S. degree in automation and informatics, the M.S. degree in automation and control engineering in the consumption industry, and the Ph.D. degree in technical cybernetics from the Tomas Bata University in Zlín, Czech Republic, in 2002, 2005, and 2013, respectively.

From 2006 to 2013, he was a Junior Lecturer with the Faculty of Applied Informatics, Tomas Bata University in Zlín, where he was a Senior Lecturer, from 2013 to 2018, and has been an Associate Professor, since 2018. He is the author of three book chapters, more than 40 journal articles, and more than 70 conference papers. His research interests include analysis, modeling, identification, and control of time-delay systems, algebraic control methods, and autotuning and optimization techniques.

Dr. PEKAŘ was a recipient of the Rector's Award for the Best Ph.D. Thesis at the Faculty of Applied Informatics, Tomas Bata University in Zlín, in 2013, and the Laureate of the ASR Seminary Instrumentation and Control, in 2007 and 2009. He was the Lead Guest Editor of *Mathematical Problems in Engineering* and *Advances in Mechanical Engineering*. Since 2018, he has been an Editor of *Mathematical Problems in Engineering*.

RADEK MATUŠŮ was born in Zlín, Czech Republic, in 1978. He received the M.S. degree in automation and control technology in consumer goods industry from the Faculty of Technology, Tomas Bata University (TBU) in Zlín, in 2002, and the Ph.D. degree in technical cybernetics from the Faculty of Applied Informatics (FAI), TBU in Zlín, in 2007.

He was appointed as an Associate Professor of machine and process control with FAI, TBU in Zlín, in 2018. He has been holding various research or pedagogical positions at TBU in Zlín, since 2004, where he is currently a Researcher and a Project Manager. His research interests include analysis and synthesis of robust control systems, fractional-order systems, and algebraic methods in control design. He has (co)authored more than 50 scientific journal articles and over 100 conference contributions.

Dr. Matušů was a Guest Editor of *Mathematic Problems in Engineering*. He has served as a Reviewer for over 40 scientific journals, including, but not limited to, *Automatica*, the IEEE Transactions on Automatic Control, and the *IEEE Control Systems Magazine*. He also serves as an Academic Editor for the *Journal of Control Science and Engineering*.